Proceedings of ICRC 2001: 1 © Copernicus Gesellschaft 2001

ICRC 2001

Gamma Ray Bursts and Cosmic Ray Origin

C. D. Dermer

Code 7653, Naval Research Laboratory, Washington, DC 20375-5352 USA

Abstract. This paper presents the theoretical basis of the fireball/blast wave model, and some implications of recent results on GRB source models and cosmic-ray production from GRBs. BATSE observations of the prompt γ-ray luminous phase, and Beppo-SAX and long wavelength afterglow observations of GRBs are briefly summarized. Derivation of spectral and temporal indices of an adiabatic blast wave decelerating in a uniform surrounding medium in the limiting case of a nonrelativistic reverse shock, both for spherical and collimated outflows, is presented as an example of the general theory. External shock model fits for the afterglow lead to the conclusion that GRB outflows are jetted. The external shock model also explains the temporal duration distribution and clustering of peak energies in prompt spectra of long-duration GRBs, from which the redshift dependence of the GRB source rate density can be derived. Source models are reviewed in light of the constant energy reservoir result of Frail et al. that implies a total GRB energy of a few $\times 10^{51}$ ergs and an average beaming fraction of $\approx 1/500$ of full sky. Paczyński's isotropic hypernova model is ruled out. The Vietri-Stella model two-step collapse process is preferred over a hypernova/collapsar model in view of the X-ray observations of GRBs and the constant energy reservoir result. Second-order processes in GRB blast waves can accelerate particles to ultra-high energies. GRBs may be the sources of UHECRs and cosmic rays with energies above the knee of the cosmic ray spectrum. High-energy neutrino and γ-ray observations with GLAST and ground-based γ-ray telescopes will be crucial to test GRB source models.

1 Introduction

In only ten years, the study of gamma-ray bursts has grown from a narrow specialty involving a small group of high-energy astronomers to a mainstream field of research that impacts nearly all topics in astronomy. This change resulted primarily from observational advances made with the Burst and Transient Source Experiment (BATSE) on the *Compton Gamma Ray Observatory*, and the discovery of X-ray afterglows and long wavelength counterparts made possible with the Beppo-SAX experiment. The BATSE results showed that the angular distribution of GRBs on the sky is isotropic, and that the GRB size distribution exhibits a strong flattening for faint bursts (Meegan et al., 1992). This behavior follows from a cosmological origin of GRB sources, with the decline in the number of faint bursts due to cosmic expansion. Follow-up X-ray observations with the Narrow Field Instruments on Beppo-SAX has permitted redshift determinations that firmly establish the distance scale to the sources of $\gtrsim 2$ s duration GRBs, which are those to which Beppo-SAX is sensitive.

The redshifts of nearly 20 GRBs are now known, with the mean redshift near unity and the largest measured redshift at $z = 4.5$. The corresponding distances imply apparent isotropic γ-ray energy releases in the range from $\approx 10^{51}$-10^{54} ergs. Recent results suggest that GRB emissions are strongly beamed, so that the total energy release is actually in the neighborhood of 10^{51} ergs, corresponding to the typical total energies released in the kinetic outflow of a supernova. Delayed reddened enhancements detected in the optical light curves of a few GRBs could also be a consequence of a supernova emission component. If the beaming results are correct, then many more sources of GRBs exist than are implied through direct statistical studies of detected GRBs. The implied rate of both aligned and misdirected GRB sources begins to approach the expected rate of Type Ib/c supernovae (SNe). These and other lines of evidence indicate that GRBs are related to a type of supernova.

This review of the theory of GRBs briefly touches on some of the central questions in contemporary GRB studies. After summarizing the prompt γ-ray luminous and delayed afterglow observations of GRBs, detections of X-ray emission line and absorption features, and some related phenomenology, the redshift distribution is presented. These redshifts are obtained from absorption lines in the optical afterglow, spec-

Correspondence to: dermer@gamma.nrl.navy.mil

troscopy of the host galaxies and, in a few cases, from X-ray line observations. Given the redshift, the directed energy releases per unit solid angle can be derived. The theoretical basis for the fireball/blast wave model is outlined, and numerical calculations derived from the model are presented. According to the blast-wave model, a central source ejects an expanding relativistic shell of particles. Accelerated electrons radiate synchrotron photons to produce the long wavelength X-ray, optical, and radio afterglows, as well as the soft γ-ray emission emitted in the prompt phase (although arguments have also been made for a Compton origin of this emission). By contrast, a synchrotron self-Compton origin may explain the > 100 MeV emission detected with EGRET from a handful of GRBs in the prompt phase, and from GRB 940217 in the afterglow phase.

The photons received during the prompt phase are emitted closest to the central source; therefore a correct theory of the origin of the prompt emission reveals properties of the central engine. We contrast an internal shock/colliding shell model with an external shock model for the prompt γ-ray emission. Beaming breaks in afterglow light curves can be used to deduce the collimation angle, and hence the true energetics of the GRB source. The most popular current model for the central sources of long-duration GRBs is the hypernova/collapsar model, where an evolved, massive star's central core collapses to a black hole while accreting material at the rate of ≈ 0.1- a few Solar masses per second. The coalescence of neutron stars and black holes has been less successful as a model for the long-duration GRBs because host galaxy evidence indicate that a massive star origin is more likely; a compact-object coalescence model may still apply to the short duration GRBs. The supranova model of Vietri and Stella invokes a two-step collapse process where the core collapse of a massive star forms a rotationally stabilized neutron star following a supernova explosion. The neutron star later collapses to form a black hole. This model has several advantages over the hypernova/collapsar model to account for the evidence of beaming and the X-ray absorption and line observations, including the presence of a highly enriched circumburster medium (CBM), and a uniform energy scale set by the mass of the neutron star.

Some important issues in GRB cosmology are mentioned, though the remainder of this review focuses on the role that GRBs may play in cosmic-ray origin studies. GRB sources release energy into an L^* galaxy such as the Milky Way at the time averaged rate of $\sim 10^{40\pm1}$ ergs s^{-1}, which is nearly equal to the cosmic ray power into our Galaxy. Relativistic blast waves can accelerate particles well beyond the knee of the cosmic-ray spectrum through second-order processes, overcoming difficulties that first-order Fermi acceleration faces to accelerate cosmic rays to energies above the knee of the cosmic ray spectrum in SNe. If the beaming results are correct, then GRBs occur in our Galaxy at the rate of once every several thousand years, suggesting that GRBs are associated with a subset of SNe. Finally, we consider high-energy neutrino production from GRBs, and show how high-energy neutrino and gamma-ray observations of GRBs can discriminate between an internal and external shock model for the prompt gamma-ray emission, with important implications for central engine theory.

2 Observations and Phenomenology

Because the emphasis here is on theory, we can only briefly summarize the basic features of GRB observations and phenomenology (for a recent review of the observations, see van Paradijs et al. (2000)). GRBs are brief flashes of radiation at hard X-ray and soft γ-ray energies that display a wide variety of time histories, though in $\sim 25\%$ of the cases a characteristic single-pulse profile is observed, consisting of a rapid rise followed by a slower decay (Fishman and Meegan, 1995). GRBs were first detected at soft γ-ray energies with wide field-of-view instruments. Peak soft γ-ray fluxes reach hundreds of photons cm^{-2} s^{-1} in rare cases. The BATSE instrument is sensitive in the 50-300 keV band, and provides the most extensive data base of GRB observations during the prompt phase. It searches for GRBs by examining strings of data for $> 5.5\sigma$ enhancements above background on the 64 ms, 256 ms, and 1024 ms time scales, and triggers on GRBs as faint as ≈ 0.5 ph cm^{-2} s^{-1}, corresponding to energy flux sensitivities $\lesssim 10^{-7}$ ergs cm^{-2} s^{-1}.

The integral size distribution of BATSE GRBs in terms of peak flux ϕ_p is very flat below ~ 3 ph cm^{-2} s^{-1}, and becomes steeper than the $-3/2$ behavior expected from a Euclidean distribution of sources at $\phi_p \gtrsim 10$ ph cm^{-2} s^{-1} (van Paradijs et al., 2000). GRBs typically show a very hard spectrum in the hard X-ray to soft γ-ray regime, with a photon index breaking from ≈ -1 at photon energies $E_{ph} \lesssim 50$ keV to a -2 to -3 spectrum at $E_{ph} \gtrsim$ several hundred keV (Band et al., 1993). Consequently, the distribution of the peak photon energies E_{pk} of the time-averaged νF_ν spectra of BATSE GRBs are typically found in the 100 keV - several MeV range (Mallozzi et al., 1995). The differential peak-flux size distribution (Meegan et al., 1996) and the E_{pk} distribution (Mallozzi et al., 1997) are shown by the data points in the top and bottom panels of Fig. 1, respectively.

The duration of a GRB is defined by the time during which the middle 50% (t_{50}) or 90% (t_{90}) of the counts above background are measured. A bimodal duration distribution is measured, irrespective of whether the t_{50} or t_{90} durations are considered (Kouveliotou et al., 1993). About two-thirds of BATSE GRBs are long-duration GRBs with $t_{90} \gtrsim 2$ s, with the remainder comprising the short-duration GRBs. The top panel of Fig. 2 shows the t_{50} duration distribution of BATSE GRBs.

The Beppo-SAX GRB observations revealed that essentially all long-duration GRBs have fading X-ray afterglows (Costa et al., 1999). The Wide Field Camera on Beppo-SAX has sensitivity down to $\sim 10^{-10}$ ergs cm^{-2} s^{-1} with $\lesssim 10'$ error boxes. Spacecraft slewing requires 6-8 hours, but permits Narrow Field Instrument X-ray observations with sensitivity down to $\sim 10^{-14}$ ergs cm^{-2} s^{-1} and error boxes $\lesssim 0.5'$. The first X-ray afterglow was obtained from GRB

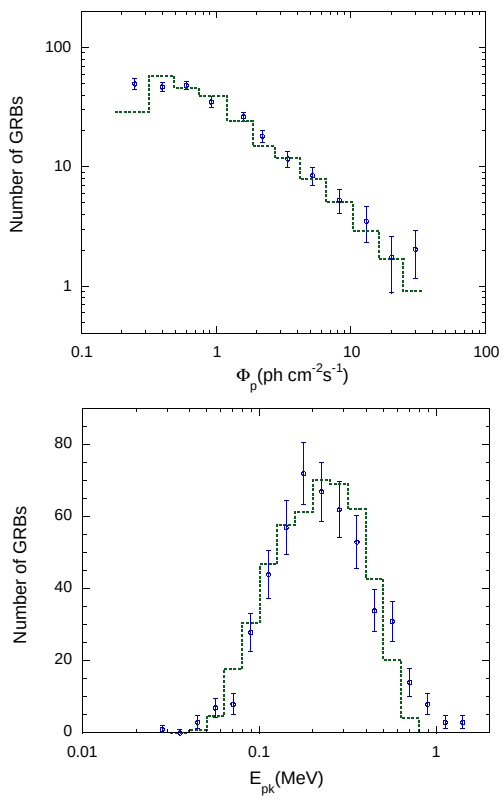

Fig. 1. Differential distribution of the number of GRBs with peak fluxes measured on the 1024 ms time scale with BATSE is plotted in the upper panel, and the distribution of the photon energies of the νF_ν peaks are plotted on the bottom panel. Histogram gives a fit to the data using an external-shock model for the prompt phase.

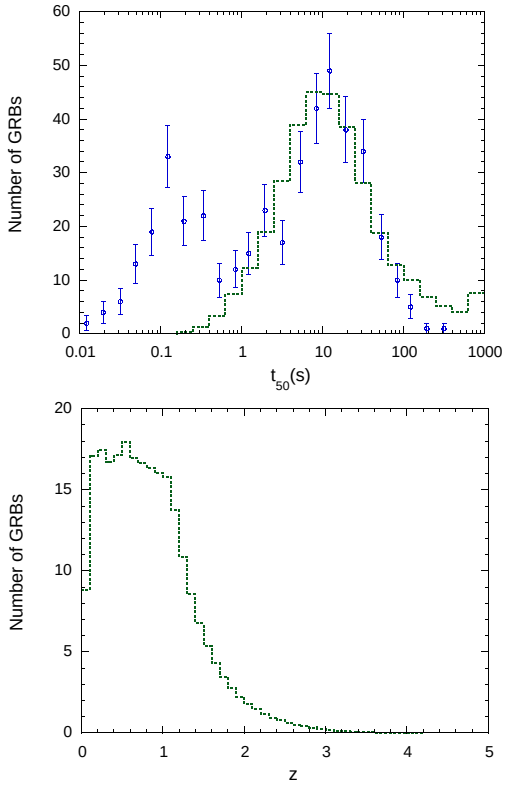

Fig. 2. Data points in the top panel give the t_{50} duration distribution. External shock-model fit to the long duration distribution is given by the histogram. Bottom panel shows the redshift distribution of BATSE GRBs predicted by the model (Böttcher and Dermer, 2000).

970228 (Costa et al., 1997), which revealed an X-ray source which decayed according to a power-law behavior $\phi_X \propto t^\chi$, with $\chi \sim -1.33$. Typically, $\chi \sim -1.1$ to -1.5 in X-ray afterglow spectra.

The small X-ray error boxes allow deep optical and radio follow-up studies. GRB 970228 was the first GRB from which an optical counterpart was observed (van Paradijs et al., 1997), and GRB 970508 was the first GRB for which a redshift was measured (Djorgovski et al., 1997; Metzger et al., 1997). Detection of optical emission lines from the host galaxy, and absorption lines in the fading optical afterglow due to the presence of intervening gas has provided redshifts for about 20 GRBs (Djorgovski et al., 2001). No optical counterparts are detected from approximately one-half of GRBs with well-localized X-ray afterglows, and are termed "dark" bursts. These sources may be undetected in the optical band because of dusty media (Groot et al., 1998). Approximately 40% of GRBs have radio counterparts, and the transition from a scintillating to smooth behavior in the radio afterglow of GRB 980425 provides evidence for an expanding source (Frail et al., 1997). Fig. 3 gives the distribution of redshift and apparent isotropic γ-ray energy releases for 17 GRB for which the redshift is known, using the compilation of Frail et al. (2001).

X-ray emission lines, possibly due to Fe Kα fluorescence, were detected during a rebrightening phase in the afterglow of GRB 970508 (Piro et al., 1999), and in the afterglow spectra of GRB 991216 (Piro et al., 2000) and GRB 000214 (Antonelli et al., 2000). A marginal detection of an X-ray emission feature was also reported from GRB 970828 (Yoshida et al., 1999). A transient absorption feature was detected from GRB 990705 (Amati et al., 2000), and X-ray absorption in excess of the Galactic hydrogen column density has also been reported in GRB 980329 (Frontera et al., 2000). These results provide an alternative method of redshift determination, and provide important clues about the environment of the progenitor object, showing that large quantities of iron must be present in the vicinity of these sources.

The EGRET instrument on the *Compton Observatory* detected 7 GRBs with > 30 MeV emission during the prompt phase (Catelli et al., 1998), including the extraordinary burst GRB 940217, which displayed $\gtrsim 100$ MeV emission 90 minutes after the onset of the GRB, including one photon with energy near 20 GeV (Hurley et al., 1994). This gives unambiguous evidence for the importance of nonthermal processes in GRBs. TeV radiation has been reported to be detected with the Milagrito water Cherenkov detector from GRB 970417a (Atkins et al., 2000). If correct, this requires that this source be located at $z \lesssim 0.3$ in order that $\gamma\gamma$ attenuation with the

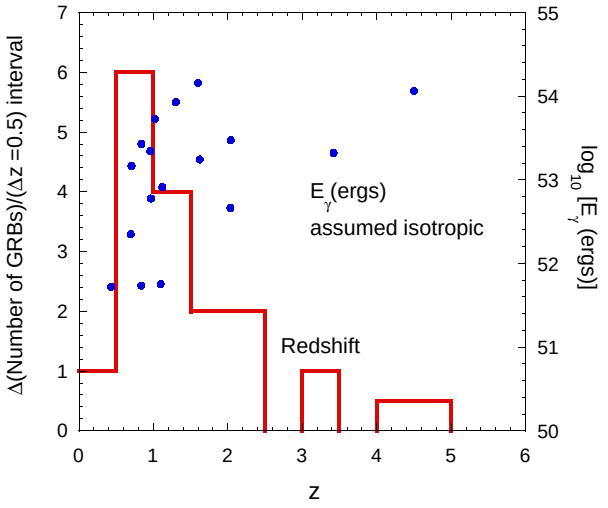

Fig. 3. Distribution of redshifts and apparent isotropic γ-ray energy releases.

diffuse intergalactic infrared radiation to be small.

A class of X-ray rich GRBs, with durations of order of minutes and X-ray fluxes in the range 10^{-8}-10^{-7} ergs cm^{-2} s^{-1} in the 2-25 keV band, has been detected with many X-ray satellites, including Ariel V, HEAO-1, ROSAT, Ginga, and Beppo-SAX (Heise et al., 2001). We also note several phenomenological correlations, including claims of an inverse correlation of luminosity and BATSE channel lags (Norris et al., 2000), correlations between the duration of quiescent and subsequent pulse periods in separated pulses (Ramirez-Ruiz et al., 2001), and indications that the peak luminosity is correlated with variability (Reichart et al., 2001). Other phenomenological behaviors in the prompt emission include hard-to-soft evolutions and hardness-intensity correlations, and a quantitative relation between integrated fluence and E_{pk} in well-defined pulses (Liang and Kargatis, 1996).

3 Elementary Blast Wave Theory

The fireball/blast-wave model for GRBs was proposed by Rees and Mészáros (1992) and Paczyński and Rhoads (1993), and successfully predicted power-law afterglows (Mészáros and Rees, 1997). It has emerged as the standard model to interpret GRB prompt and afterglow emissions (for a recent review, see Mészáros (2002)). The simplest version of the standard blast wave model involves a spherical, uncollimated explosion taking place in a uniform surrounding medium. A relativistic pair fireball is formed when an explosion deposits a large amount of energy into a compact volume. The pressure of the explosion causes the fireball to expand, with the thermal kinetic energy of the explosion being transformed into directed kinetic energy due to strong adiabatic cooling of particles in the comoving frame (Mészáros et al., 1993; Piran, 1999). Because of the Thomson coupling between the particles and photons, most of the original explosion energy is carried by the baryons that were originally mixed into the explosion. Under certain conditions involving less energetic, temporally extended, or very baryon-clean explosions, neutrons can decouple from the flow (Derishev et al., 1999). If this does not occur, then the coasting Lorentz factor $\Gamma_0 \cong E_0/M_b c^2$, where M_b is the baryonic mass and $E_0 = 10^{52} E_{52}$ ergs is the apparent isotropic energy release.

In the simplest version of the model, the blast wave is approximated by a uniform thin shell, and particle acceleration is assumed to take place at the forward shock only. A forward shock is formed when the expanding shell accelerates the external medium, and a reverse shock is formed due to deceleration of the cold shell. The forward and reverse shocked fluids are separated by a contact discontinuity and have equal kinetic energy densities. From the relativistic shock jump conditions (Sari and Piran, 1995), $4\Gamma(\Gamma-1)n_0 = 4\bar{\Gamma}(\bar{\Gamma}-1)n'_{sh}$, where Γ is the blast wave Lorentz factor, $\bar{\Gamma}$ is the Lorentz factor of the reverse shock in the rest frame of the shell, n'_{sh} is the density of the unshocked fluid in the proper frame of the expanding shell, and n_0 is the density of the CBM, here assumed to be composed of hydrogen. Particle acceleration at the reverse shock is unimportant when the reverse shock is nonrelativistic, which occurs when

$$\Gamma \ll \sqrt{\frac{n'_{sh}}{n_0}} \ . \qquad (1)$$

The unique feature of GRBs is that the coasting Lorentz factor Γ_0 may reach values from hundreds to thousands. By contrast, Type Ia and II SNe have ejecta speeds that are in the range of $\sim$ 5000-30000 km s^{-1}. The relativistic motion of the radiating particles introduce many interesting effects in GRB emissions that must be properly taken into account.

Three frames of reference are considered when discussing the emission from systems moving with relativistic speeds: the stationary frame, which are denoted here by asterisks, the comoving frame, denoted by primes, and the observer frame. The differential distance traveled by the expanding blast wave during differential time dt_* is simply $dx = \beta c dt_*$, where $\beta = \sqrt{1-\Gamma^{-2}}$. Due to time dilation, $dx = \beta\Gamma c dt'$. Because of time dilation, the Doppler effect, and the cosmological redshift z, the relationship between comoving and observer times is $(1+z)\Gamma dt'(1-\beta\cos\theta) = (1+z)dt'/\delta = dt$, where θ is the angle between the emitting element and the observer and $\delta = [\Gamma(1-\beta\cos\theta)]^{-1}$ is the Doppler factor. For on-axis emission from a highly relativistic emitting region, we therefore see that $dt \cong (1+z)dx/\Gamma^2 c$; consequently the blast wave can travel a large distance $\Gamma^2 c\Delta t$ during a small observing time interval. A photon measured with dimensionless energy $\epsilon = h\nu/m_e c^2$ is emitted with energy $\delta\epsilon'/(1+z)$.

A blast wave expanding into the surrounding medium acts as a fluid if there is a magnetic field in the comoving frame sufficiently strong to confine the particles within the width of the blast wave. The blast-wave width depends on the duration of the explosion and the spreading of the blast-wave particles. Because sub-second structure is regularly observed in GRB light curves, the central engine must be $\lesssim 1$ lt-s,

and is probably much thinner in view of 1-10 ms variability observed in some GRBs (Bhat et al., 1992). We denote this length scale by Δ_0 cm. The shell will spread radially in the comoving frame by an amount $x'_{\parallel} \simeq v_{spr}t'$, where $t' \cong x/(\beta\Gamma c)$ is the available comoving time and v_{spr} is the spreading speed. This implies a shell width in the observer frame of $\Delta = x/\Gamma_0^2$ due to length contraction, and a spreading radius $x_{spr} = \Gamma_0^2\Delta_0$, assuming that the shell spreads with speed $v_{spr} \cong c$. The width of the unshocked blast-wave fluid in the rest frame of the explosion is therefore $\Delta = \min(\Delta_0, x/\Gamma_0^2)$ (Mészáros et al., 1993; Sari et al., 1996). Milligauss fields are sufficient to confine relativistic electrons.

As the blast wave expands, it sweeps up material from the surrounding medium to form an external shock (Mészáros and Rees, 1993). In a colliding wind scenario, the blast wave intercepts other portions of the relativistic wind (Rees and Mészáros, 1994). Protons captured by the expanding blast wave from the CBM will have total energy $\Gamma m_p c^2$ in the fluid frame, where m_p is the proton mass. The kinetic energy swept into the comoving frame by an uncollimated blast wave at the forward shock per unit time is given by

$$\frac{dE'}{dt'} = 4\pi x^2 n_0 m_p c^3 \beta\Gamma(\Gamma - 1) \tag{2}$$

(Blandford and McKee, 1976). One factor of Γ represents the increase of external medium density due to length contraction, the factor $(\Gamma - 1)$ is proportional to the kinetic energy of the swept up particles, and the factor β is proportional to the rate at which the particle energy is swept. Thus the power is $\propto \Gamma^2$ for relativistic blast waves, and $\propto \beta^3$ for nonrelativistic blast waves. This process provides internal energy available to be dissipated in the blast wave.

A proton that is captured by and isotropized in the comoving frame will have energy $\Gamma m_p c^2$ in the comoving fluid frame, or energy $\Gamma^2 m_p c^2$ in the observer frame. The expanding shell will therefore begin to decelerate when $E_0 = \Gamma_0 M_b c^2 = \Gamma_0^2 m_p c^2 (4\pi x_d^3 n_0/3)$, giving the deceleration radius

$$x_d \equiv (\frac{3E_0}{4\pi\Gamma_0^2 c^2 m_p n_0})^{1/3} \cong 2.6\times 10^{16}(\frac{E_{52}}{\Gamma_{300}^2 n_0})^{1/3}\ \mathrm{cm} \tag{3}$$

(Rees and Mészáros, 1992; Mészáros and Rees, 1993), where $\Gamma_{300} = \Gamma_0/300$. Acceleration at the shock front can inject power-law distributions of particles. In the process of isotropizing the captured particles, magnetic turbulence is introduced (Pohl and Schlickeiser, 2000) that can also accelerate particles to very high energies through a second-order Fermi process.

The deceleration time as measured by an on-axis observer is given by

$$t_d \equiv (1+z)\frac{x_d}{\beta_0\Gamma_0^2 c} \cong \frac{9.6\ (1+z)}{\beta_0}\ (\frac{E_{52}}{\Gamma_{300}^8 n_0})^{1/3}\ \mathrm{s}\ . \tag{4}$$

The factor $\beta_0^{-1} = 1/\sqrt{1-\Gamma_0^{-2}}$ generalizes (Dermer and Humi, 2001) the result of Mészáros and Rees (1993) for mildly relativistic and nonrelativistic ejecta, as in the case of Type Ia and Type II supernova explosions. The Sedov radius

$$\ell_{\rm S} = \Gamma_0^{2/3} x_d = (\frac{3E_0}{4\pi m_p c^2 n_0})^{1/3} \cong \tag{5}$$

$$1.2\times 10^{18}(\frac{E_{52}}{n_0})^{1/3}\ \mathrm{cm}\ \cong 6.6\times 10^{18}(\frac{m_\odot}{n_0})^{1/3}\ \mathrm{cm}\ ,$$

where $m_\odot$ is the total (rest mass plus kinetic) explosion energy in units of Solar rest mass energy. For relativistic ejecta, $\ell_{\rm S}$ refers to the radius where the blast wave slows to mildly relativistic speeds, i.e., $\Gamma \sim 2$. The Sedov radius of a SN that ejects a 10 $M_\odot$ envelope could reach ~ 5 pc or more. The Sedov age $t_{\rm S} = \ell_{\rm S}/v_0 \cong 700(m_\odot/n_0)^{1/3}/(v_0/0.01c)$ yr for nonrelativistic ejecta, and is equivalent to t_d in general.

The evolution of an adiabatic blast wave in a uniform surrounding medium for an explosion with a nonrelativistic reverse shock is given by (Dermer and Humi, 2001)

$$P(x) = \frac{P_0}{\sqrt{1+(x/x_d)^3}} \cong \begin{cases} \beta_0\Gamma_0\ , & x \ll x_d \\ \beta_0(\frac{x}{\ell_{\rm S}})^{-3/2}\ , & x_d \ll x \end{cases}\ , \tag{6}$$

where $P = \beta\Gamma$ and $P_0 = \beta_0\Gamma_0$ represent dimensionless bulk momenta of the shocked fluid. Equation (6) reduces to the adiabatic Sedov behavior for nonrelativistic ($\beta_0\Gamma_0 \ll 1$) explosions, giving $v \propto x^{-3/2}$, $x \propto t^{2/5}$, and $v \propto t^{-3/5}$, as is well-known. In the relativistic ($\Gamma_0 \gg 1$) limit, $\Gamma \propto x^{-3/2}$ and $t \cong c^{-1}\int dx/\Gamma^2 \propto \int dx\, x^3$, yielding $x \propto t^{1/4}$ and $\Gamma \propto t^{-3/8}$ when $\Gamma \gg 1$. The adiabatic behavior does not apply when radiative losses are important. A nonrelativistic supernova shock becomes radiative at late stages of the blast-wave evolution. It is not clear whether a GRB fireball is highly radiative or nearly adiabatic during either its gamma-ray luminous prompt phase or during the afterglow (Waxman, 1997; Vietri, 1997). In the fully radiative limit, equation of energy conservation gives $\beta_0\Gamma_0 M_0 \cong \beta\Gamma[M_0 + 4\pi n_0 x^3/3]$, giving the asymptotes $\Gamma \propto x^{-3}$ when $\Gamma_0 \gg \Gamma \gg 1$ and $\beta \propto x^{-3}$ when $\Gamma - 1 \ll 1$.

Most treatments employing blast-wave theory to explain the observed radiations from GRBs assume that the radiating particles are electrons. The problem here is that $\sim m_p/m_e \sim 2000$ of the nonthermal particle energy swept into the blast-wave shock is in the form of protons or ions unless the surroundings are composed primarily of electron-positron pairs (Königl and Granot, 2001). For a radiatively efficient system, physical processes must therefore transfer a large fraction of the swept-up energy to the electron component. In elementary treatments of the blast-wave model, it is simply assumed that a fraction e_e of the forward-shock power is transferred to the electrons, so that

$$L'_e = e_e\frac{dE'}{dt'}\ . \tag{7}$$

If all the swept-up electrons are accelerated, then joint normalization to power and number gives

$$\gamma_{min} \cong e_e(\frac{p-2}{p-1})(\frac{m_p}{m_e})(\Gamma - 1)\ \cong e_e k_p(\frac{m_p}{m_e})\Gamma \tag{8}$$

for $2 < p < 3$, where the last expression holds when $\Gamma \gg 1$ and $k_p = (p-2)/(p-1)$.

The strength of the magnetic field is another major uncertainty. The standard prescription is to assume that the magnetic field energy density $u_b = B^2/8\pi$ is a fixed fraction e_B of the downstream energy density of the shocked fluid. Hence

$$\frac{B^2}{8\pi} = 4 e_B n_0 m_p c^2 (\Gamma^2 - \Gamma) \ . \tag{9}$$

It is also generally supposed in simple blast-wave model calculations that some mechanism – probably the first-order shock Fermi process – injects electrons with a power-law distribution between electron Lorentz factors $\gamma_{min} \leq \gamma \leq \gamma_2$ downstream of the shock front. The electron injection spectrum in the comoving frame is modeled by the expression

$$\frac{dN'_e(\gamma)}{dt' d\gamma} = K_e \gamma^{-p} \ , \ \text{for} \ \gamma_{min} < \gamma < \gamma_2 \ , \tag{10}$$

where K_e is normalized to the rate at which electrons are captured.

The maximum injection energy is obtained by balancing synchrotron losses and an acceleration rate given in terms of the inverse of the Larmor time scale through a parameter e_2, giving

$$\gamma_2 \cong 4 \times 10^7 e_2 / \sqrt{B(\mathrm{G})} \ . \tag{11}$$

A break is formed in the electron spectrum at cooling electron Lorentz factor γ_c, which is found by balancing the synchrotron loss time scale t'_{syn} with the adiabatic expansion time $t'_{adi} \cong x/\Gamma c \cong \Gamma t \cong t'_{syn} \cong (4 c \sigma_{\rm T} B^2 \gamma_c / 24\pi m_e c^2)^{-1}$, giving

$$\gamma_c \cong \frac{3 m_e}{16 e_B n_0 m_p c \sigma_T \Gamma^3 t} \tag{12}$$

(Sari et al., 1998). For an adiabatic blast wave, $\Gamma \propto t^{-3/8}$, so that $\gamma_{min} \propto t^{-3/8}$ and $\gamma_c \propto t^{1/8}$.

The observed νF_ν synchrotron spectrum from a GRB depends on the geometry of the outflow. Denoting the comoving spectral luminosity by $L'_{syn}(\epsilon') = \epsilon'(dN'/d\epsilon' dt')$, then $\epsilon' L'_{syn}(\epsilon') \cong \frac{1}{2} u_B c \sigma_{\rm T} \gamma^3 N_e(\gamma)$, with $\gamma = \sqrt{\epsilon'/\epsilon_B}$ and $\epsilon_B = B/B_{cr} = B/(4.41 \times 10^{13}$ G). For a spherical blast-wave geometry, the spectral power is amplified by two powers of the Doppler factor δ for the transformed energy and time. The νF_ν synchrotron spectrum is therefore

$$f_\epsilon^{syn} \cong \frac{2\Gamma^2}{4\pi d_L^2} \, (u_B c \sigma_{\rm T}) \, \gamma^3 N'_e(\gamma) \ , \ \gamma \cong \sqrt{\frac{(1+z)\epsilon}{2\Gamma \epsilon_B}} \ . \tag{13}$$

where d_L is the luminosity distance.

For collimated blast waves with jet opening angle θ_j, equation (13) does not apply when $\Gamma \lesssim 1/\theta_j$ because portions of the blast wave's radiating surface no longer contribute to the observed emission. In this case, the blast-wave geometry is a localized emission region, and the received νF_ν spectrum is given by

$$f_\epsilon^{syn} \cong \frac{\delta^4}{4\pi d_L^2} \, (\frac{1}{2} u_B c \sigma_{\rm T}) \, \gamma^3 N'_e(\gamma) \ , \ \gamma \cong \sqrt{\frac{(1+z)\epsilon}{\delta \epsilon_B}} \ . \tag{14}$$

Here the observed flux is proportional to four powers of the Doppler factor: two associated with solid angle, one with energy and one with time.

From this formalism, analytic and numerical models of relativistic blast waves can be constructed. It is useful to define two regimes depending on whether $\gamma_{min} < \gamma_c$, which is called the weak cooling regime, or $\gamma_{min} > \gamma_c$, called the strong cooling regime (Sari et al., 1998). If the parameters p, e_e and e_B remain constant during the evolution of the blast wave, then a system originally in the weak cooling regime will always remain in the weak cooling regime. In contrast, a system in the strong cooling regime will evolve to the weak cooling regime.

For a power-law injection spectrum given by equation (10), the cooling comoving nonthermal electron spectrum can be approximated by

$$N'_e(\gamma) \cong \frac{N_e^0 \, \gamma_0^{s-1}}{s-1} \begin{cases} \gamma^{-s} \ , & \gamma_0 \lesssim \gamma \lesssim \gamma_1 \\ \gamma_1^{p+1-s} \gamma^{-(p+1)} \ , & \gamma_1 \lesssim \gamma \lesssim \gamma_2, \end{cases} \tag{15}$$

and $N_e^0 = 4\pi x^3 n_0/3$ for the assumed system. In the weak cooling regime, $s = p$, $\gamma_0 = \gamma_{min}$ and $\gamma_1 = \gamma_c$, whereas in the strong cooling regime, $s = 2$, $\gamma_0 = \gamma_c$ and $\gamma_1 = \gamma_{min}$.

As an example of the elementary theory, consider the temporal index in the strongly cooled regime for high energy electrons with $\gamma \geq \gamma_1 = \gamma_m \propto \Gamma$, $\gamma_0 = \gamma_c \propto 1/(\Gamma^3 t)$, and $s = 2$. From equation (13), $f_\epsilon \propto \Gamma^4 x^3 \, \gamma_0^{s-1} \gamma_1^{p+1-s} \epsilon^{(2-p)/2} / \Gamma^{2-p} \propto \Gamma^{2(p-1)} x^3 \epsilon^{(2-p)/2} / t \propto t^\chi \epsilon_\nu^\alpha$, with $\chi = (2-3p)/4$ and $\alpha_\nu = (2-p)/2$. A few other such results include the decay of a strong and weak cooling νF_ν peak frequency $\epsilon_{pk} \propto t^{-3/2}$ and $\epsilon_{pk} \propto t^{-3p/2}$, resepctively. A cooling index change by $\Delta(\alpha_\nu) = 1/2$ is accompanied by a change of temporal index from $\chi = 3(1-p)/4$ to $\chi = (2-3p)/4$ at late times, so that $\Delta\chi = 1/4$. Extension to power-law radial electron profiles is obvious, and beaming breaks introduce two additional factors of Γ from $\delta \approx \Gamma$ in equation (14) when the observer sees beyond the causally connected regions of the jetted blob, noting that N_e^0 must be renomalized appropriately.

Fig. 4 shows spectral and temporal indices that are derived from the preceding analytic considerations of a spherical adiabatic blast wave that is in the strong cooling regime during a portion of its evolution (Dermer and Böttcher, 2002). We use the notation that the νF_ν spectrum is described by

$$f_\epsilon \propto t^\chi \epsilon^{\alpha_\nu} \ . \tag{16}$$

Observations at a specific photon energy ϵ will detect the system evolving through regimes with different spectral and temporal behaviors. The relativistic Sedov phase corresponds to the afterglow regime, and we also consider in this figure a possible relativistic reverse shock (RRS) phase. If equation

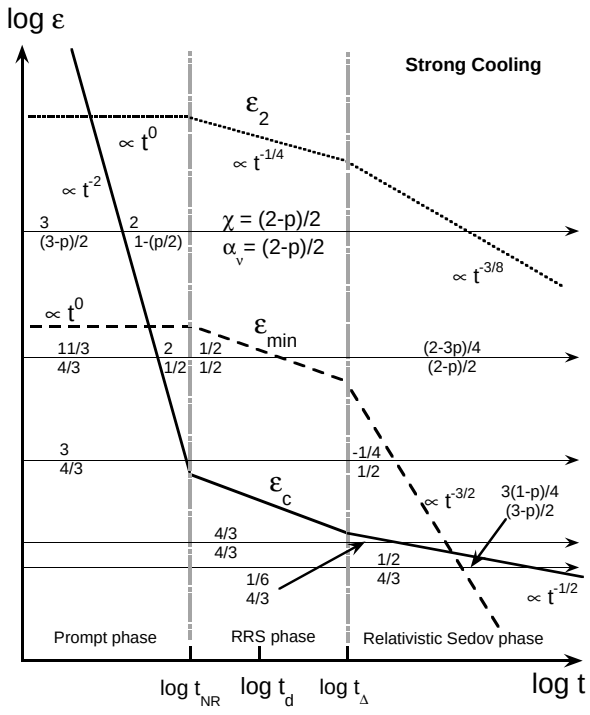

Fig. 4. Possible time profiles and spectral behavior of the nonthermal synchrotron radiation that could arise for a system that is in the fast cooling regime during a portion of the adiabatic evolution of a blast wave in a uniform surrounding medium. The temporal indices χ and νF_ν spectral indices α_ν are shown, respectively, above and below the lines that represent different families of possible emission trajectories.

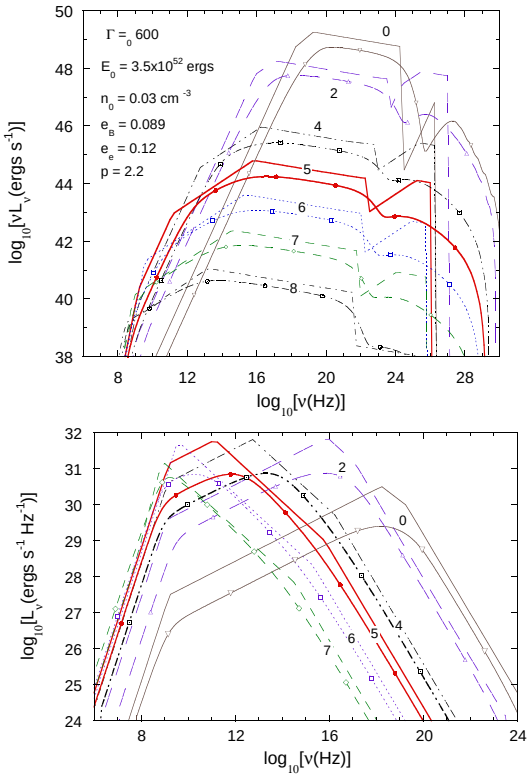

Fig. 5. Calculations of spectral energy distributions emitted by a relativistic blast wave with initial Lorentz factor $\Gamma_0 = 600$ that is energized by sweeping up material from a uniform surrounding medium with density n. Curves are labeled by the base 10 logarithm of the observing time in seconds. The analytic and numerical models are shown, with the latter curves identified by data points. Other parameters of the calculation are shown in the legend, based on parameters taken from the fit to GRB 970508 by Wijers and Galama (1999). Upper panel shows spectral energy distribution in a νL_ν representation, and the lower panel shows light curves at different energies in an L_ν representation.

(1) is satisfied with Γ replaced by Γ_0, then the blast wave will not evolve through the RRS phase. Even for this simple system, a wide variety of behaviors are possible. Inclusion of additional effects, including a nonuniform external medium (Mészáros et al., 1998) or blast-wave evolution in a partially radiative phase (Böttcher and Dermer, 2000a) will introduce additional complications.

The heavy solid and dotted lines in Fig. 4 represent the evolution of the cooling photon energies ϵ_c and ϵ_{min}, respectively. In the lower-right hand corner of the diagram, one sees that observations in the afterglow phase may detect a transition from the uncooled portion of the synchrotron spectrum where $\chi = (3-p)/2$ and $\alpha_\nu = (3-p)/2$ to a cooled portion of the synchrotron spectrum where $\chi = (2-3p)/4$ and $\alpha_\nu = (2-p)/2$. Thus a change in photon index by 0.5 units is accompanied by a change in temporal index by 1/4 unit, independent of p. Comparison with afterglow observations can be used to test the blast-wave model (Galama et al., 1998). The upcoming Swift telescope will be able to monitor behaviors in the time interval between the prompt and afterglow phase, and to search for other regimes of blast wave evolution and evidence for evolution in the non-adiabatic regime.

Fig. 5 shows a numerical model of a relativistic blast wave calculated with the code developed by Chiang and Dermer (1999), which takes into account light travel-time delays from different portions of the blast wave, synchrotron and synchrotron self-Compton emission, as well as self-absorption. The numerical results are compared with analytic spectral energy distributions (Dermer et al., 2000) in which an SSC component is included in the approach of Sari et al. (1998). We use parameters derived by Wijers and Galama (1999) to fit afterglow data from GRB 970508. Here the total energy injected into the fireball is $E = 3.5 \times 10^{52}$ ergs, and the density of the external medium is $n = 0.03$ cm^{-3}. The SSC component becomes increasingly important with increasing e_e/e_B (Sari et al., 1996; Moderski et al., 2000), and will be observed as features in the X-ray and optical light curves (Dermer et al., 2000a; Zhang and Mészáros, 2001). As can be seen, the analytic expressions provide a reasonable representation of the numerical model in the optical/X-ray regime, but the discrepancies at radio frequencies are significant, as is clear from the second panel in Fig. 5. Although the times of the temporal breaks arising from synchrotron emission emitted by the lowest energy electrons are in good agreement with the numerical calculation, the analytic model can be dis-

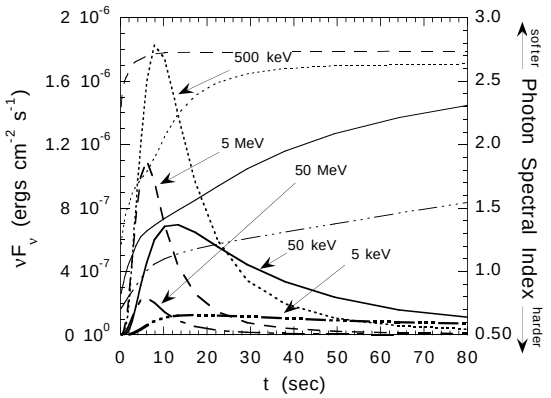

Fig. 6. Numerical calculations of light curves measured at different observed photon energies. These profiles correspond to the most common prompt GRB light curves. The hard-to-soft evolution is indicated by the variation in the photon index. For this model, an explosion with total energy $E_0 = 10^{54}$ ergs and coasting Lorentz factor $\Gamma_0 = 300$ expands into a uniform surrounding medium with density $n_0 = 100$ cm^2.

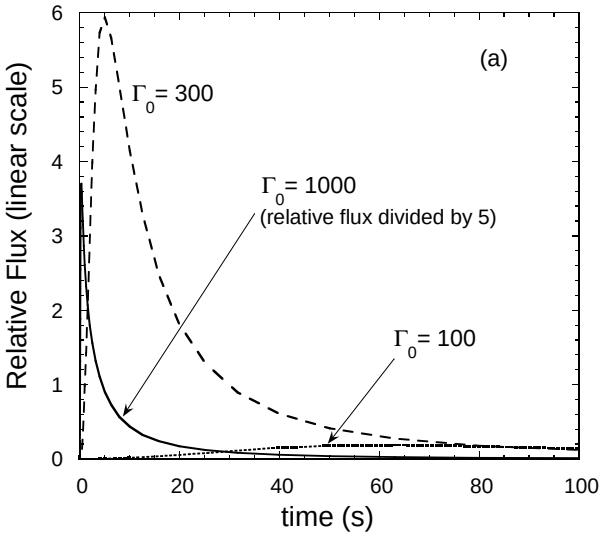

Fig. 7. Light curves calculated at 100 keV from a fireball with other parameters the same as in Fig. 6.

crepant in flux values by an order-of-magnitude or more, so that any quantitative statement based upon analytic models must be made with care, particularly in the radio regime.

Fig. 6 shows light curves calculated from an adiabatic blast wave that expands into a uniform surrounding medium (Dermer et al., 1999b). The light curves display a temporal profile that rapidly rises and slowly decays, and reproduces the so-called fast-rise, exponential decay profiles observed in a significant fraction of GRBs. This indicates that the prompt emission in these GRBs, at least, arises from an external shock model. An external shock origin also accounts for the basic phenomenology of the GRBs with smooth profiles, including the hard-to-soft evolution and the hardness-intensity correlation observed in GRB light curves.

3.1 Clean and Dirty Fireballs

If a subset of prompt GRB light curves originate from an external shock model in the prompt phase, one might ask what this means for the remainder of the GRBs. A majority of the GRB community believes that an active central engine is required to reproduce the spiky, short timescale variablity observed in a large number of GRB light curves, and that an impulsive explosion cannot produce the temporal gaps detected in some GRB light curves. Inhomogeneities in the surrounding medium can, in fact, produce short timescale variability and gaps in the light curves, as demonstrated by Dermer and Mitman (1999). More serious issues for the external shock model for the prompt emission are posed by the observations of optical emission observed in GRB 990123 in the prompt phase if due to reverse shock emission (Akerlof et al., 1999), and the correlated durations of quiescent and subsequent peak durations in GRB light curves (Ramirez-Ruiz et al., 2001).

Rather than revisit this controversy, it seems more useful to focus on the predictive capability of the external shock model. Because of the small number of parameters, it is simple to outline the generic behavior of GRBs in terms of the model's most sensitive parameters, namely the total explosion energy E_0, the surrounding medium density n_0, and the coasting Lorentz factor Γ_0.

The basic features of GRB fireballs can be summarized by a few simple equations (Dermer et al., 1999a). The first is that the total energy liberated in photons during the prompt phase is

$$E_\gamma \cong 0.1\ \Pi_0 t_d\ , \tag{17}$$

where the precise value of the coefficient, here taken to be 10%, depends on how radiative the fireball is during this phase. The power Π_0 during the prompt phase is

$$\Pi_0 \propto (n_0 E_0^2)^{1/3}\ \Gamma_0^{8/3} \tag{18}$$

and, as already seen in equation (4), the deceleration time

$$t_d \propto (\frac{E_0}{n_0})^{1/3}\ \Gamma_0^{-8/3}\ . \tag{19}$$

Most of the emission during the prompt phase is radiated at photon energy

$$E_{pk} \propto n_0^{1/2} \Gamma_0^4\ . \tag{20}$$

The strong dependence of these quantities on Γ_0 is evident. A detector observing in a fixed range of photon energy centered at E_{det}, such as BATSE, will have strong selection biases to detect fireballs with different Γ_0 factors. The biases against detecting dirty fireballs, namely those with small values of Γ_0 and large baryon-loading, arise because the peak luminosity measured by a detector declines rapidly when $\Gamma_0 \lesssim \bar{\Gamma}_0$. The quantity $\bar{\Gamma}_0$ is the Lorentz factor of a fireball that produces the bulk of its emission near the sensitive range of a detector, and is defined by $E_{pk} = E_{det} \propto$

$n_0^{1/2}\bar{\Gamma}_0^4$, where E_{det} is the photon energy to which the GRB detector is largest effective area. The peak luminosity is larger for clean fireballs with $\Gamma_0 > \bar{\Gamma}_0$ and small baryon loading, but the shorter durations of the clean events mean that detectors trigger on fluence rather than peak flux when $\Gamma_0 \gg \bar{\Gamma}_0$. GRB detectors are therefore also biased against the detection of clean fireballs. This explains the tendency of detectors to detect GRBs that produce prompt radiation with νF_ν peak in the waveband at which the detector has greatest sensitivity.

These considerations resolve the apparent paradox that a beamed scenario should seem to produce a wide range of E_{pk}, contrary to observations (Dermer et al., 1999b) (see lower panel in Fig. 1). To avoid fine-tuning of Γ_0, one realizes that there must be two additional classes of explosive phenomena that remain to be discovered by detectors with appropriate design (Dermer et al., 1999a), namely the large baryon-load, low Γ_0 "dirty" fireballs, and the low baryon-load, high Γ_0 "clean" fireballs.

This is apparent from Fig. 7, which shows how a variation of a factor of 3 in Γ_0 from 300 to 100 can make a GRB essentially undetectable in the BATSE band. The low Lorentz factor, dirty fireballs are more extended in time, and radiate their energy at lower observed photon frequencies. These may correspond to the X-ray rich GRBs that have been detected with Beppo-SAX and previous X-ray detectors (Heise et al., 2001).

By taking the triggering properties of BATSE into account, the external shock model can be used to fit the statistical data on GRBs (Böttcher and Dermer, 2000). The results are shown in Figs. 1 and 2, where simple power-law distributions of Γ_0 and E_0 were assumed. The underlying assumption of this model is that the rate of GRBs per comoving density follows the star formation history of the universe. These results show that fine-tuning is not required to explain the tendency of E_{pk} to be within a narrow range. The tendency of softer bursts to have longer durations is a direct consequence of this model, though only the long duration GRBs are fit in this model. A wide range of apparent isotropic energy releases E_0 is used to fit the statistical data. If GRBs are beamed, the distribution of E_0 would be consistent with recent analyses that indicates that GRBs have a standard energy reservoir, with the apparent variation of E_0 reflecting the range of jet opening angles.

3.2 Beaming in GRBs

An observer will receive most emission from those portions of a GRB blast wave that are within an angle $\sim 1/\Gamma$ to the direction to the observer. As the blast wave decelerates by sweeping up material from the CBM, a break in the light curve will occur when the jet opening half-angle θ_j becomes smaller than $1/\Gamma$. This is due to a change from a spherical blast wave geometry, given by equation (13), to a geometry defined by a localized emission region, as given by equation (14). Assuming that the blast wave decelerates adiabatically in a uniform surrounding medium, the condition $\theta_j \cong 1/\Gamma =$

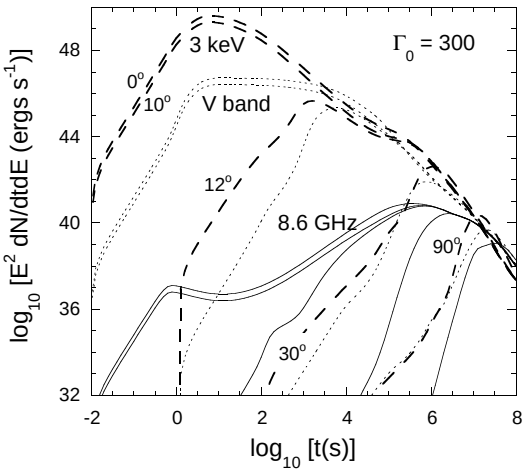

Fig. 8. Light curves calculated at various observing energies and inclination angles θ for a fireball with parameters the same as in Fig. 6 and jet opening half-angle $\theta_j = 10^\circ$. The dashed, dotted, and solid curves give light curves measured at 3 keV, V band, and 8.6 GHz radio frequencies, and the observing angles $\theta = 0^\circ, 10^\circ, 12^\circ, 30^\circ$, and 90°.

$\Gamma_0^{-1}(x_{br}/x_d)^{3/2} = \Gamma_0^{-1}(t_{br}/t_d)^{3/8}$ implies

$$t_{br} \approx 45(1+z)\,(\frac{E_{52}}{n_0})^{1/3}\theta_j^{8/3}\ \mathrm{days}\ , \tag{21}$$

from which the jet angle

$$\theta_j \approx 0.1[\frac{t_{br}(\mathrm{d})}{1+z}]^{3/8}\,(\frac{n_0}{E_{52}})^{1/8} \tag{22}$$

can be derived (Sari et al., 1999). Note that the beaming angle is only weakly dependent on n_0 and E_0.

Fig. 8 shows calculations of a GRB blast wave in a beamed geometry (Dermer et al., 2000a) with $\theta_j = 10^\circ$ at different observing angles and energies. The jet emission is assumed to be uniform across its surface and not to spread laterally (see Rhoads (1999) when this is not the case). For the parameters used here ($E_{52} = 100$, $e_B = 10^{-4}$, $e_e = 0.5$, $n_0 = 100$ cm^{-3}, $p = 2.5$), the beaming break occurs at $\sim 10^5$ s, but is obscured at X-ray and optical frequencies by the appearance of an SSC component. The appearance of clearly defined breaks in the light curves of some GRBs, if due to beaming rather than to a variation in the density of the surrounding medium, limits the ratio e_e/e_B that defines the strength of the SSC component (Dermer et al., 2000a). So-called "orphan" afterglows, which are those GRBs with jets pointed away from our line-of-sight which become visible upon deceleration of the blast wave, may be confused with dirty fireballs (Dermer et al., 2000a; Huang, et al., 2002).

Afterglow modeling of multiwavelength spectra of GRB 980703, GRB 990123, GRB 9905010, and GRB 991216 by

Panaitescu and Kumar (2001) shows that the CBM is more consistent with uniform surroundings than with a wind profile with density $n(r) \propto r^{-2}$. They derive magnetic field parameters in the range $10^{-4} \lesssim e_B \lesssim 0.05$, electron energy-transfer parameters in the range $0.01 \lesssim e_e \lesssim 0.1$, and obtain low density surroundings ($\sim 10^{-4} \lesssim n_0 \lesssim 10\,\mathrm{cm}^{-3}$) in their fits. The jet angles θ_j range from 1° to 4°. The beaming factor for a one-sided jet is $\approx 1.3\times10^4/(\theta^\circ)^2$, so that many misaligned GRBs sources should exist for every detected GRB.

Frail et al. (2001) have considered a larger sample of GRBs and show that the beaming results provide evidence for a standard energy reservoir. Letting η_γ represent the efficiency for transforming total energy E_{tot} (which should be distinguished from the apparent isotropic energy release E_0) to γ ray energy, then $E_{tot} \simeq \theta_j^2 E_\gamma(\mathrm{iso})/(4\eta_\gamma)$, where $E_\gamma(\mathrm{iso})$ is the apparent isotropic energy release in the form of GRBs. They find that the mean energy release by the GRB sources is $\langle E_{GRB}\rangle \cong 3\times10^{51}/(\eta_\gamma/0.2)$ ergs, and that the actual event rate of GRBs is $\approx 500\times$ the observed rate. If correct, this result has important implications for the nature of the sources of GRBs.

4 Source Models

Keeping in mind that only members of the class of long-duration GRBs have measured redshifts, considerable evidence connects GRBs to star-forming regions (Djorgovski et al., 2001; Sokolov et al., 2001) and, consequently, to a massive star origin. For example, the associated host galaxies have blue colors, consistent with galaxy types that are undergoing active star formation. GRB counterparts are found within the optical radii and central regions of the host galaxies (Bloom, et al., 1999a). Lack of optical counterparts in some GRBs could be due to extreme reddening from large quantities of gas and dust in the host galaxy (Galama and Wijers, 2001). Supernova-like emissions have been detected in the late-time optical decay curves of a few GRBs (Reichart, 1999; Bloom, et al., 1999b), and X-ray evidence for Fe Kα-line signatures indicates that large quantities of highly enriched material are near the sources of GRBs. The spatial and temporal coincidence of GRB 980425 with SN 1998bw, a Type Ic supernova, if true, also connects the sources of GRBs to SNe (Kulkarni et al., 1998; Pian et al., 1999).

4.1 Coalescing Compact Objects

A central attraction of this model is that binary neutron stars, such as the Hulse-Taylor pulsar PSR 1913+16, exist. This system has a merger time scale $\approx 3\times10^8$ yrs, which is much less than the Hubble time, so that these events undoubtedly occur. The timescale for the final coalescence event is very short, with the bulk of the energy released over a few tens of milliseconds (Janka et al., 1999). Such events should, however, occur in both spiral and elliptical galaxies, whereas the host galaxies of known GRBs generally exhibit active star formation and are therefore associated with spiral or disturbed galaxy hosts. The absence of counterparts far from the disks of galaxy hosts also conflicts with this model, as such old stellar systems can travel great distances before coalescence. In particular, they should leave dusty regions where young and massive stars are born.

Merger-rate estimates of neutron-star/neutron-star in addition to neutron-star/black-hole binaries range from $\approx 10^{-5}$-10^{-6} yr^{-1} in our Galaxy, but are quite uncertain due to the sensitive dependence of merging timescale on initial binary separation (Narayan et al., 1991; Tutukov and Yungelson, 1993). Even so, if GRBs outflows are highly beamed, event rates $\gtrsim 10^{-4}$ yr^{-1} are implied (see §6.3). Taken together, these various lines of evidence do not support a model of coalescing compact objects for the long duration GRBs.

4.2 Hypernova/Collapsar Model

In the original formulation of this model (Woosley, 1993), a collapsar was a "failed" supernova in the sense that a core-collapse event failed to collapse to form a neutron star and instead produced a black hole. In order to produce a long-duration GRB with complex pulse structure, Woosley (1993) argued that accretion had to proceed over a period of time comparable to the prompt phase of a GRB. The progenitor star was suggested to be a rotating Wolf-Rayet star that produces, upon collapse, an accretion disk of several tenths of Solar masses. Because of the accretion geometry, jetted emission from neutrino annihilation was formed along the axis of the system.

Paczyński (1998) introduced the word "hypernova" to refer to the extremely luminous prompt GRB and afterglow events, and concurred with Woosley that GRBs are formed by the collapse of a massive star to a black hole surrounded by a massive disk and torus. He also suggested that the precursor X-ray emission observed with Ginga in several GRBs (Murakami et al., 1991) was a signature of a dirty fireball produced as the ejecta cleared away overlying baryonic material, after which a highly relativistic, clean fireball could then emerge. In the version of the hypernova model advanced by Paczyński (1998), the events are in fact as energetic as 10^{54} ergs and 10^4-10^5 times rarer than SNe.

Hydrodynamical simulations of collapsars have specifically treated, for example, the evolution of a 35 $M_\odot$ main-sequence star whose 14 $M_\odot$ helium core collapses to form a 2-3 $M_\odot$ black hole (MacFadyen and Woosley, 1999). Provided that the core has a large amount of angular momentum, a delayed accretion event can be formed by the infalling matter. The black-hole jet simulation is performed by injecting $\sim 10^{51}$ ergs s^{-1}, which is argued to be generated by magneto-hydrodynamical processes rather than neutrino annihilation, insofar as the latter process produces inadequate energy to break through the core. In cases where breakthrough is not possible, a choked event is formed, which could in principle be detected from neutrino observations (Mészáros and Waxman, 2001). A distinction is made between prompt and delayed collapse to a black hole, with black-hole production occurring in the latter case due to de-

layed fallback onto a young neutron star (MacFadyen et al., 2001).

The collapsar model must contend with the difficulty of ejecting baryon-clean material through an overlying shell of material. This is accomplished through an active central engine that persists for at least as long as the prompt phase of the GRB. Formation of relativistic jets of baryonic-clean material reaching $\Gamma_0 \sim 10^2$-10^3 represents a major difficulty in these models (Tan et al., 2001).

4.3 Supranova Model

A central motivation of the supranova model of Vietri and Stella (1998) is to identify a site that is originally free of baryon contamination. This occurs through a two-step collapse to a black hole, where a "supramassive" neutron star (i.e., with mass exceeding the Chandrasekhar limit) is formed in the first-step through a supernova explosion. The neutron star is initially stabilized against collapse by rotation. The loss of angular momentum support through magnetic dipole and gravitational radiation leads to collapse to a black hole after some months to years. A two-step collapse process means that the neutron star is surrounded by a supernova shell of enriched material which can explain rebrightening events, as seen in GRB 970508 (Vietri et al., 1999). Alternately, the neutron star could be driven to collapse by accreting matter in a binary system (Vietri and Stella, 1999).

The period of activity of a highly magnetized neutron star preceding its collapse to a black hole can produce a pulsar wind bubble consisting of low density, highly magnetized pairs (Königl and Granot, 2001), in accord with afterglow model fits (Panaitescu and Kumar, 2001). The earlier supernova could yield $\sim 1 M_\odot$ of Fe in the surrounding vicinity. The discovery of variable Fe absorption in GRB 990705 during the prompt emission phase (Amati et al., 2000) and X-ray emission features in the afterglow spectra of GRB 991216 (Piro et al., 2000) provide a test of this model. Variable X-ray absorption is essentially undetectable from a GRB surrounded by a uniform CBM, even if highly enriched (Böttcher et al., 1999). Extremely clumped ejecta (Böttcher et al., 2002) or blueshifted resonance scattering in a high-velocity outflow (Lazzati et al., 2001) can account for the variable absorption.

Fig. 9 illustrates the allowed parameter space in the supranova model, where f refers to the volume filling factor of the ejecta. By contrast, collapsar progenitors must produce $\gtrsim 0.1 M_\odot$ of iron within ~ 1 pc, but massive stars that have metal rich winds lose too much mass to form a collapsar (Fryer, 2001). A He-merger model, where a binary compact object merges with the He core of a companion, requires an unreasonably short merger timescale (Böttcher et al., 2002).

4.4 Other Models

These three classes of models hardly exhaust the possibilities. Some alternative suggestions include a strong-field millisecond pulsar origin, where the collapse of a white dwarf to a neutron star produces an $\sim 10^{15}$ Gauss magnetar with a millisecond period (Usov, 1992, 1994). Others include the "cannonball" model (Dar and De Rújula, 2000) involving highly relativistic and highly beamed jets of materials from SNe. Another involves the transition of a neutron star in a low-mass binary X-ray system to a strange star (Cheng and Dai, 1996). In others, a pair electromagnetic pulse (Ruffini et al., 2001) or the Blandford-Znajek effect (Lee et al., 2000) extract the energy during the black-hole formation event.

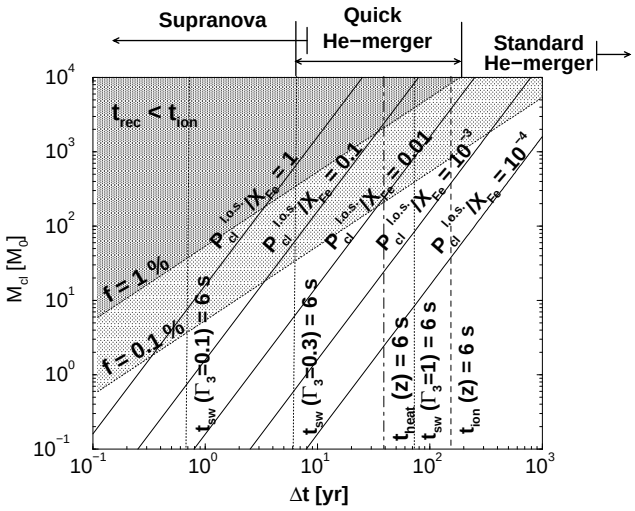

Fig. 9. Parameter space giving the amount of supernova ejecta mass M_{cl} that must be concentrated in clumps versus the time delay Δt between the primary supernova explosion and the subsequent GRB to explain the variable absorption feature in GRB 990705 (Böttcher et al., 2002). Solid lines give the probability P_{cl}^{los} that a clump will be along the line of sight, which depends on the iron enhancement X_{Fe} with respect to Solar system values. The vertical dotted lines refer to GRB blast wave Lorentz factors $\Gamma_0 = 1000\Gamma_3$ that give results consistent with the observations.

4.5 Best-Bet Model

In light of the Fe line observations and the constant energy reservoir result of Frail et al. (2001), the supranova model seems to offer certain advantages over a collapsar model to explain the origin of GRBs. For example,

1. The narrow distribution of energy releases follows from a progenitor model involving neutron stars that collapse to black holes, since the neutron-star progenitor masses must be very similar. By contrast, a large diversity of core masses is possible in the collapsar model, and the varying mantle structure would strongly modulate the energy radiated as γ rays.

2. The immediate environment is much cleaner in the vicinity of a collapsing neutron star than in a massive-star collapsar model. Thus the baryon-contamination problem is more easily solved in the supranova model.

3. The production of large amounts of iron in the GRB environment is possible in a two-step collapse process,

with the delay between the first- and second-step event permitting the nickel and cobalt to decay to iron prior to the GRB.

4. The lack of evidence for winds from massive stars and the low surrounding densities is contrary to expectations in a model where GRBs originate in the direct collapse of massive stars to black holes (Panaitescu and Kumar, 2001). Moreover, the low densities inferred for the surroundings are much less than expected for typical ISM environment, and could be expected in pulsar wind bubbles (Königl and Granot, 2001).

5. The typical E_{pk} energies observed in BATSE can be explained in a prompt external shock model, which is compatible with the prompt collapse of a neutron star to a black hole in the supranova model. The narrow distribution of E_{pk} energies seems to require fine tuning in a model with internal shocks in a relativistic wind, and no argument from first principles has been advanced to explain the typical durations of the long-duration GRBs in a collapsar wind model.

The evidence is not yet compelling to rule out either model; for example, iron line observations can be explained in the context of the collapsar model through a persistent source of emission involving either a magnetar or the delayed accretion onto a black hole (Rees and Mészáros, 2000; Mészáros and Rees, 2001). By contrast, the delay between neutron star formation and collapse to a black hole in the supranova model seems to require ad hoc assumptions about the spin rates and magnetic fields of the neutron stars formed in SNe explosions. Various anisotropic and clumpy ejecta are required. If GRB history is any guide, the best bet is on a model yet to be proposed.

5 Gamma Ray Burst Cosmology

We mention some of the main lines of research in GRB cosmology, making no claims for completeness. The rate of lensing events on GRBs can set limits to the cosmological abundance of dark matter in the form of compact objects, depending on the specific cosmology (Marani et al., 1999). High-redshift GRBs provide probes of the early universe that can be used to examine the redshift dependence of metallicity, the onset of the first generation of stars, the evolution of Lyα forest and metal absorption line systems, and the epoch of reionization (Lamb and Reichart, 2000; Ciardi and Loeb, 2000). An interesting feature of the afterglow is that its brightness is not strongly dependent on redshift. The metallicity also may depend on the location of the GRB source in the host galaxy (Ramirez-Ruiz et al., 2002). X-ray obscuration of high-redshift GRBs and the fraction of optically dark bursts will reveal whether GRBs are hosted in luminous infrared galaxies similar to the high-redshift SCUBA galaxies (Ramirez-Ruiz et al., 2002a).

Totani (1997, 1999) and Wijers et al. (1998) showed that if GRB sources have a massive star origin, then the redshift distribution of GRBs yields the star formation rate (SFR) history of the universe. Gamma rays are less attenuated during transport than optical radiation, so that a complete sample of GRB redshifts will arguably give a better measure of the SFR than measurements inferred from optical and UV surveys of galaxies, which are subject to strong extinction corrections.

Before a large number of GRB redshifts were known, it was first necessary to determine whether the BATSE count rate distribution was in accord with the assumption that the rate of GRBs followed the SFR history, as inferred, for example, from HST observations (Madau et al., 1998). This depends sensitively on the assumed luminosity function of GRBs. Krumholz et al. (1998) demonstrated, however, that a variety of luminosity and redshift distributions of cosmological GRBs are consistent with the observed peak flux distribution, so that a GRB rate density distribution that followed the SFR of the universe was not unique. The degeneracy of the unknown GRB luminosity function can be broken by assuming a specific model for GRB emission, as done by Böttcher and Dermer (2000) for an external shock model. This leads to a specific prediction for the redshift distribution of GRBs (Fig. 2, lower panel) based upon the assumed SFR function, and the GRB energy and Lorentz factor distributions. Comparison with GRB redshift data can then be used to refine the model parameters and test the basic assumption that the rate density of GRBs follows the SFR of the universe.

GRBs can have important effects on the galaxy environment, and were proposed as the energy sources of HI shells and stellar arcs (Efremov et al., 1998; Loeb and Perna, 1998), though the evidence for beaming makes these possibilities less likely. GRBs could melt dust grains by GRB UV radiation to produce flash-heated chondrules in the early Solar system (McBreen and Hanlon, 1999). In one sense, the most cosmologically interesting effect of GRBs is their influence on biological activity (Scalo and Wheeler, 2002) and life extinction (Dar and De Rújula, 2001), which depends not only on GRB photon production but on particles accelerated by GRBs, namely cosmic rays.

6 Cosmic Ray Production by GRBs

As summarized in §4, several lines of evidence indicate that GRBs are closely related to a subset of SNe that drives a relativistic outflow in addition to the nonrelativistic ejecta expelled during the collapse of the massive core to a neutron star. The relativistic ejecta decelerate to nonrelativistic speeds at the Sedov radius by sweeping up matter from the external medium. Particle acceleration occurs at these shocks, just as in the nonrelativistic shocks from "normal" Type Ia and Type II supernova remnants, though with the addition of a relativistic phase of deceleration. The first-order shock Fermi mechanism is generally recognized as the mechanism that accelerates GeV/nuc cosmic rays in the converging flows formed by the forward shock. In addition, second-order Fermi acceleration of particles through gyroresonant particle-wave interactions with magnetic turbulence gener-

ated in the shocked fluid can also accelerate particles to high energies.

We consider the simplest case of particle acceleration via the first- and second-order Fermi processes at the external shock formed by ejecta decelerating in a uniform surrounding medium. These considerations will establish whether GRBs can accelerate particle to the ankle of the cosmic ray spectrum at 3×10^{18}-10^{19} eV and to ultra-high ($> 10^{19}$ eV) energies. We show that ultra-high energy cosmic rays (UHECRs) can in principle be accelerated by GRB blast waves. Additional effects involving internal shocks, acceleration at the reverse shock, or a highly magnetized CBM can improve the acceleration efficiency.

6.1 Constraints on Acceleration

A basic requirement for particle acceleration to some maximum energy E_{max} in the observer frame is that the Larmor radius $r'_{\rm L}$ be smaller than the comoving size scale r' of the system. The comoving Larmor radius $r'_{\rm L} = mc^2\gamma/qB$ for particles with mass $m = Am_p$ and charge $q = ze$. The requirement that $r'_{\rm L} \leq r'$ implies that

$$E_{max,{\rm L}} = \frac{qB\Gamma\delta ct_{var}}{1+z} \cong 10^{18}\ \frac{ZB({\rm G})\Gamma^2_{300}t_{var}({\rm s})}{1+z}\ {\rm eV}\ , \quad (23)$$

where r' is related to the measured variability timescale t_{var} through the relation $t_{var} \cong (1+z)t'_{var}/\delta \cong (1+z)r'/c\delta$, and $\delta \approx \Gamma$. Recalling from equation (9) that $B \cong 116\sqrt{e_B n_0}\Gamma_{300}$ G, we see that UHECR acceleration can be achieved for highly relativistic GRB outflows, especially if large Z nuclei such as iron are accelerated.

In Fermi processes, particles can increase their energy by $\sim mc^2\gamma$ on a Larmor timescale $t_{\rm L} = 2\pi r_{\rm L}/c = 2\pi mc\gamma/qB$ (Rachen and Mészáros, 1998). Hence the maximum acceleration rate is $\dot\gamma_{acc} = f_{acc}(qB/2\pi mc)$, where $f_{acc} \lesssim 1$. A basic constraint on particle acceleration is the radiation reaction limit due to synchrotron losses. The synchrotron loss rate

$$-\dot\gamma_{syn} = \frac{4}{3}c\sigma_{\rm T}\ (\frac{B^2}{8\pi m_e c^2})\ \frac{Z^4}{(m/m_e)^3}\ \gamma^2\ . \quad (24)$$

Equating this with $\dot\gamma_{acc}$ gives the radiation-reaction limit on particle acceleration through Fermi processes

$$E_{max,syn} = mc^2\Gamma\ \sqrt{\frac{3ef_{acc}}{\sigma_{\rm T}B}}\ \frac{(m/m_e)}{Z^{3/2}} \quad (25)$$

This gives $E_{max,syn} \approx 6 \times 10^{15}\Gamma_{300}\sqrt{f_{acc}/B({\rm G})}$ eV for electrons, and a maximum synchrotron photon energy $h\nu_{max} \cong 20 f_{acc}\Gamma$ MeV, independent of B, as is well-known (de Jager et al., 1996). For ions, the synchrotron radiation-reaction limiting energy is

$$E_{max,syn\ ion} = 2.4 \times 10^{22}\frac{A^2}{Z^{3/2}}\Gamma_{300}\sqrt{\frac{f_{acc}}{B({\rm G})}}\ {\rm eV} \quad (26)$$

The maximum ion synchrotron photon energy is $h\nu_{max} \cong 40(Af_{acc}/Z^2)\Gamma$ GeV. Other processes, such as Compton losses for leptons and photomeson and photopair losses for ions, can limit acceleration further. Provided that these losses are not severe, the synchrotron radiation reaction is not a severe limitation for UHECR particle acceleration.

Another kinematic limitation on first-order Fermi acceleration arises from the size scale of the system. Because particles must be scattered upstream of the shock, the upstream Larmor radius $r_{\rm L}$ must be smaller than the characteristic size of the system during the period when the shock is strong. The Sedov radius, given by equation (5), is the radius where the blast wave has swept up an amount of matter equal to the ejecta mass. Particle acceleration is strongly suppressed after the explosion enters the Sedov regime. The condition $r_{\rm L} < \ell_{\rm S}$ implies that

$$E_{max,size} \approx 2 \times 10^{15} Z\ B_{\mu{\rm G}}\ (\frac{m_\odot}{n_0})^{1/3}\ {\rm eV} \quad (27)$$

where the $B_{\mu{\rm G}}$ and n_0 are the mean magnetic field, in μG, and density of the interstellar medium.

The time required to cycle across the supernova shock provides a further limitation on particle acceleration by shock Fermi processes. The first-order Fermi acceleration rate $\dot\gamma_{FI} \approx \beta\gamma/t_{cyc}$, where β is the shock speed, and the cycle time

$$t_{cyc} \cong \frac{4}{c}(\frac{\kappa_-}{u_-} + \frac{\kappa_+}{u_+})\ \approx \frac{\eta r_{{\rm L},-}}{\beta c}\ . \quad (28)$$

Here κ is the diffusion coefficient, u is the speed of the flow in the rest frame of the shock, and subscripts $-$ and $+$ refer to quantities upstream and downstream of the shock, respectively (e.g., Drury, 1983; Kirk, 1994). The expression on the right-hand-side assumes that the time to scatter is determined by quantities upstream of the shock, and that the diffusion coefficient is given by the Bohm diffusion limit $\eta r_{{\rm L},-}$. Differences in cycle times from quasi-parallel and quasi-perpendicular shocks arise from shock-drift in the latter case. The maximum energy-gain rates per unit distance x for nonrelativistic quasi-parallel and quasi-perpendicular shocks, respectively, are given by

$$\frac{dE'}{dx}|_{\parallel,max} \simeq \beta qB_-\ \ ;\ \ \frac{dE'}{dx}|_{\perp,max} \simeq \beta^{2/3}qB_-\ \ . \quad (29)$$

The energy increases by only a factor $\cong 2$ in a single cycle following the first cycle in relativistic shock acceleration (Gallant and Achterberg, 1999).

By integrating the energy-gain rate over the equation of blast wave evolution given by equation (6), the classic result of Lagage and Cesarsky (1983) is generalized to give the maximum particle energy

$$E_{max,I} \approx 10^{16} Z B_{\mu{\rm G}}\beta_0^{2/3}(\frac{m_\odot\Gamma_0}{n_0})^{1/3}\ {\rm eV} \quad (30)$$

that can be obtained by first-order Fermi acceleration at a forward external shock. This shows that neither nonrelativistic or relativistic first-order shock-Fermi processes are capable of accelerating particles to the ankle of the cosmic ray spectrum. In fact, nonrelativistic ($\beta_0\Gamma_0 \ll 1$) shocks have

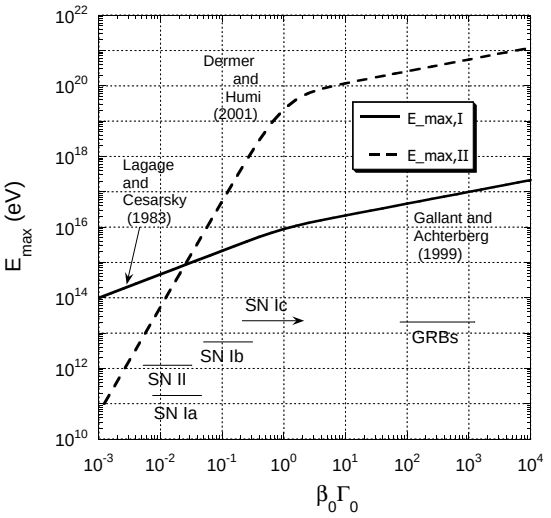

Fig. 10. Maximum proton energies from first- and second-order Fermi acceleration for explosions with initial Lorentz factors Γ_0 and speed $\beta_0 c$.

difficulties to accelerate particles past the knee of the spectrum (Lagage and Cesarsky, 1983), although winds from the pre-supernova star can enhance the local magnetic field and reduce the surrounding medium density and so permit acceleration to much higher energies (Völk and Biermann, 1988).

Second-order Fermi acceleration from gyroresonant interactions between particles and waves in relativistic shocks can accelerate particles to considerably higher energies than first-order Fermi acceleration when the wave speeds approach c. For a wave spectrum composed of Alfven waves with speed $v_{\rm A}$, the acceleration rate from a power law spectrum of waves $w(k) \propto k^{-v}$ with wavenumber $k > k_{min}$ is given by

$$\dot{\gamma}_{FII} \approx (\frac{v_{\rm A}}{c})^2 \xi (v-1)\ (\frac{c}{r_{\rm L}^0})(r_{\rm L}^0 k_{min}\gamma)^{v-1}\ . \qquad (31)$$

Here $r_{\rm L}^0 = mc^2/qB$ is the nonrelativistic Larmor radius, and v is the index of the turbulence spectrum ($v = 5/3$ corresponds to a Kolmogorov spectrum). Magnetic field turbulence is produced in the relativistic shocked fluid when particles and dust are captured and isotropized (Pohl and Schlickeiser, 2000; Schlickeiser and Dermer, 2000). After integrating over the energy gain rate during the duration of a decelerating blast wave, one obtains a maximum particle energy

$$E_{max,II} \approx 8 \times 10^{20} Z K_v e_B^{1/2} n_0^{1/6} f_\Delta \beta_0 (m_\odot \Gamma_0)^{1/3}\ {\rm eV} \qquad (32)$$

(Dermer, 2001), where $K_v \cong [0.6 e_B \beta_0 \xi / f_\Delta]^{1/(2-v)}$ for $v = 3/2{,}5/3$, and $f_\Delta x/\Gamma^2 \cong x/12\Gamma^2$ gives the observer frame width of the blast wave from the shock-jump conditions in a uniform CBM (Vietri, 1998, 1995; Panaitescu et al., 1998; Dermer and Humi, 2001). The strong dependence of the maximum energy on β_0 makes second-order processes unimportant in nonrelativistic flows when $\beta_0 \ll 0.1$.

Fig. 10 compares the maximum proton energies that can be obtained by first-and second-order Fermi acceleration at an external shock formed by an explosion with total energy $m_\odot = 1$, corresponding to 1.8×10^{54} ergs. The surrounding external medium contains a 1 μG field and a density of 1 cm^{-3}. A fully turbulent magnetic field with $\xi = 1$, $e_B = 0.2$, and $v = 3/2$ is assumed in the second-order process. First-order Fermi processes cannot accelerate particles to ultra-high energies for particles accelerated from low energies for typical ISM conditions. Relativistic shocks can, however, give a pre-existing relativistic particle population a single-cycle boost by a factor Γ^2 (Gallant and Achterberg, 1999; Vietri, 1995).

6.2 UHECR by GRBs

The Larmor radius of a particle with energy $10^{20} E_{20}$ eV is $\approx 100 E_{20}/(Z B_{\mu{\rm G}})$ kpc. Unless UHECRs are heavy nuclei, it is unlikely that they originate from our Galaxy. The proposal that UHECRs are accelerated by extragalactic GRB sources was first advanced by Vietri (1995), Waxman (1995), and Milgrom and Usov (1995). The first two of these authors noted that the energy density of UHECRs was comparable to the energy density that would be produced by GRB sources within the GZK radius, assuming that the γ-ray and UHECR power from GRBs are roughly equal. Although the details of this estimate are incorrect inasmuch as they were made before the Beppo-SAX results on the detailed redshift distribution of GRBs, the overall energy-density estimate still gives strong circumstantial support for this hypothesis.

The argument proceeds by noting that the energy density of UHECRs observed near Earth is simply

$$u_{UH} \cong \zeta\ \frac{L_{GRB} t_{esc}}{V_{prod}} \qquad (33)$$

where L_{GRB} is the power of GRBs throughout the production volume V_{prod} of the universe. UHECRs are produced with an efficiency ζ compared with the γ-ray power and "escape" from the universe primarily through photohadronic processes with an effective escape time t_{esc}.

The mean γ-ray fluence of BATSE GRBs is $F_\gamma \approx 3 \times 10^{-6}$ ergs cm^{-3} and their rate over the full sky is $\dot{N}_{GRB} \approx 2$/day. If most GRBs are at redshift $\langle z \rangle \sim 1$, then their mean distance is $\langle d \rangle \approx 2 \times 10^{28}$ cm, so that the average isotropic energy release of a typical GRB source is $\langle E_\gamma \rangle \approx 4\pi \langle d \rangle^2 F_\gamma/(1+z) \cong 8 \times 10^{51}$ ergs, implying a mean GRB power into the universe of $L_{GRB} \approx 2 \times 10^{47}$ ergs s^{-1}. (This estimate is independent of the beaming fraction, because a smaller beaming fraction implies a proportionately larger number of sources.) UHECR protons lose energy due to photomeson processes with CMB photons in the reaction $p + \gamma \to p + \pi^0, n + \pi^+$. The effective distance for 10^{20} eV protons to lose 50% of their energy is 140 Mpc (Stanev et al., 2000), so that $t_{esc} \cong 1.5 \times 10^{16}$. This implies that the energy density observed locally is $u_{UH} \approx 10^{-22} \eta$ ergs cm^{-3}. By comparing with Fig. 11, we see that this estimate is about an order of magnitude below the energy density of super-GZK particles with energies exceeding 10^{20} eV.

Given the limitations of this crude estimate, the coincidence between the GRB power and the UHECR energy den-

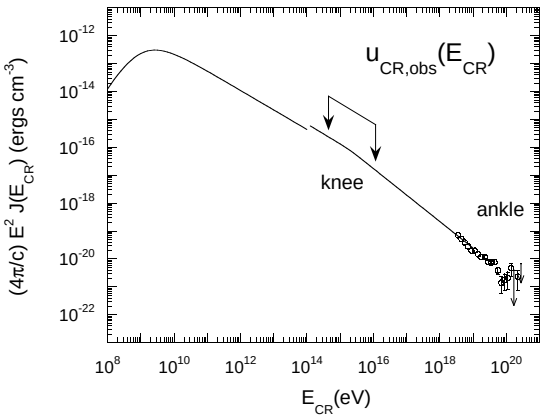

Fig. 11. Cosmic ray energy density observed near Earth. The two solid curves show extrapolations to model fits of the observed cosmic-ray proton (Simpson, 1983) and all-particle (Fowler et al., 2000) spectrum, and the data points are UHECR observations from AGASA (Takeda et al., 1998).

sity suggests that this hypothesis may be correct if GRBs can accelerate UHECRs with high efficiency ($\eta \approx 1$). An improved estimate must consider several other aspects, including

1. The efficiency of GRB sources to produce γ-ray emission within the BATSE band. If only 10% of the total energy of GRBs are radiated at soft γ-ray energies, then these sources will be much more energetic on average, which will improve the comparison – provided that UHECR acceleration remains very efficient.

2. The actual redshift distribution of GRB sources. If the rate density of GRB sources follows the SFR history of the universe (Madau et al., 1998), then the local comoving rate density will be $\approx$ 6-10 times less than the rate density at $z \approx 1$. This effect, when factored into our improved knowledge of the GRB redshift distribution showing that the faintest GRBs are at $z > 1$, makes the hypothesis that UHECRs are accelerated by GRBs more difficult to sustain (Stecker, 2000).

3. The existence of the dirty and clean fireball classes of GRBs. These sources classes would not trigger BATSE, and the dirty fireball class could be detected as the X-ray rich GRBs (Heise et al., 2001). This correction could increase the average power into the universe by a factor $\sim 3-5$ (Dermer, 2000).

4. The uncertainty in the energy density of the super-GZK cosmic rays. The UHECR energy density shown in Fig. 11 is from the AGASA measurements. Monocular HiRes observations show a lower flux than AGASA above $\approx 10^{20}$ eV by a factor of ≈ 5 (Sommers, 2002), which improves the coincidence between the UHECR energy density and the GRB power.

A detailed estimate of GRB power is given by Dermer (2000) in the context of an external shock model for GRBs performed by Böttcher and Dermer (2000). The conclusion of this study is that GRBs remain a viable source origin for UHECRs. A testable prediction of the hypothesis is that star-forming galaxies which host GRB activity will be surrounded by neutron-decay halos (Dermer, 2000), as discussed in §7.

6.3 Rate and Power of GRBs in the Milky Way

The preceding estimates were made for extragalactic sources of cosmic rays. GRBs will also take place in galaxies such as our own. After a relativistic GRB blast wave decelerates to nonrelativistic speeds, it evolves in a manner similar to nonrelativistic supernova remnant shocks. GRBs will therefore power cosmic rays with energies below the knee of the cosmic ray spectrum. These cosmic rays will add to cosmic rays accelerated in the remnants of Type I and Type II SNe. Here we estimate the rate and power of GRBs throughout the Milky Way in order to determine the contribution of GRBs to cosmic ray production.

We assume the constant energy reservoir result of Frail et al. (2001) to estimate the rate of GRBs into L^* galaxies such as the Milky Way. The local density of L^* galaxies can be derived from the Schechter luminosity function, and is $\approx 1/(200\text{-}500\ \mathrm{Mpc}^3)$ (Wijers et al., 1998; Scalo and Wheeler, 2002; Dermer, 2000). The BATSE observations imply, as already noted, ~ 2 GRBs/day over the full sky. Due to beaming, this rate is increased by a factor of $500 f_{500}$, where $f_{500} \sim 1$. Given that the volume of the universe is $\sim 4\pi(4000\ \mathrm{Mpc})^3/3$, this implies a rate per L^* galaxy of

$$\rho_{L^*} \approx \frac{300\ \mathrm{Mpc}^3/L^*}{\frac{4\pi}{3}(4000\ \mathrm{Mpc})^3}\ \frac{2}{\mathrm{day}}\ \frac{365}{\mathrm{yr}} \times 500 f_{500} \times SFR \times K_{FT}$$

$$\approx 2\times 10^{-4}\ (\frac{SFR}{1/6}) \times (\frac{K_{FT}}{3}) \times f_{500}\ \mathrm{yr}^{-1}\ . \qquad (34)$$

The factor SFR corrects for the star-formation activity at the present epoch. The SFR rate per comoving volume is about 1/6 as active now as it was at $z = 1$, and the factor K_{FT} accounts for dirty and clean fireball transients that are not detected as GRBs. Thus a GRB occurs about once every 5000 years throughout the Milky Way.

Table 1 gives the outflow speeds and rates of different types of SNe and GRBs in the Galaxy. The data for the outflow speeds of Types Ia, II, and Ib/c come from Lozinskaya (1992) and Weiler et al. (2000). The mean values of the initial dimensionless momentum $\langle\beta_0\Gamma_0\rangle$ of the outflows are also given. The supernova rate data are obtained by multiplying the results of Cappellaro et al. (1999) for galaxies of Type Sbc-Sd (renormalized by Panagia (2000) to an H-band luminosity for $h_{70} = 1$) by a factor of 2 to account for the luminosity of the Milky Way. One sees that the GRB rate is about 10% as frequent as Type Ib/c SNe, and about 1% as frequent as Type II SNe. The rates of dirty and clean fireballs are unknown, but if the X-ray rich γ-ray bursts comprise the tail of the dirty fireball population, then they could

Table 1. Ejecta Speeds and Rates of Supernovae and GRBs in the Milky Way

Explosion Type	Outflow Speed (km s^{-1})	$\langle\beta_0\Gamma_0\rangle$	Rate (century^{-1})
SN Ia	$\lesssim 2\times10^4$	0.03	0.42
SN II	$\sim 10^3$-2×10^4	0.01	1.7
SN Ib/c	$\sim 1.5\times10^3$-2×10^5	0.2	0.28
Dirty	3×10^5	30	?
GRB	3×10^5	300	~ 0.02
Clean	3×10^5	3000	?

be even more frequent than the GRB population. Statistical fits (Böttcher and Dermer, 2000) to the BATSE data suggest that the rate of clean fireballs is smaller than the GRB rate.

By weighting the GRB rate, equation (34), by the mean energy of $3\times10^{51}/(\eta_\gamma/0.2)$ ergs, we see that the time-averaged power of GRBs throughout the Milky Way or other L_* galaxies is

$$L_{MW} \approx 2\times10^{40}\frac{f_{500}}{(\eta_\gamma/0.2)}\,(\frac{SFR}{1/6})\,(\frac{K_{FT}}{3})\ \mathrm{ergs\ s^{-1}}\ . \quad (35)$$

Because each GRB has a total energy release of a few $\times10^{51}$ ergs, comparable to SNe, but occur $\sim$ 100 times less frequently, the available power from the sources of GRBs is only a few per cent of the power from Type Ia and Type II SNe. This would suggest that GRB sources can only make a minor contribution to cosmic ray production below the ankle, but the efficiency for accelerating cosmic rays in the nonrelativistic SN outflows could be considerably less than in the relativistic outflows of GRBs.

In this regard, note that Cas A has recently been detected with HEGRA at TeV energies at the level of $\approx 8\times10^{-13}$ ergs cm^{-2} s^{-1} (Aharonian et al., 2001). Spectral considerations suggest that the emission is hadronic. The expected level of 100 MeV- TeV γ-ray production can be estimated to be

$$F_\gamma \approx (4\pi d^2)^{-1}\times10^{51}\ \mathrm{ergs}\ \eta_p\times c\sigma_{pp}n_0 \approx$$

$$7\times10^{-11}\,(\frac{\eta_p}{0.1})\,n_0\,(\frac{d}{3.4\ \mathrm{kpc}})^{-2}\ \mathrm{ergs\ cm^{-2}\ s^{-1}}\ , \quad (36)$$

where the strong interaction cross section $\sigma_{pp}\approx 30$ mb. This expression may underestimate the spectral energy flux measured at a fixed frequency range and the γ-ray production efficiency, but unless the density is unusually tenuous in the vicinity of Cas A and other SNRs examined with the Whipple telescope (Buckley et al., 1998), the TeV observations suggest that most SNRs do not accelerate cosmic rays with high efficiency.

The hypothesis that cosmic rays are accelerated by SNRs is favored in view of the power provided by SNe (Gaisser, 1990). With an energy release of $\sim 10^{51}$ ergs per SN and a rate of ≈ 1 every 30 years, the power into the Galaxy from SNe is at the level of $\approx 10^{42}$ ergs s^{-1}, well in excess of the $\approx 5\times10^{40}$ ergs s^{-1} required to power GeV/nuc cosmic rays. Moreover, first-order Fermi acceleration by a strong shock produces a -2 spectrum, similar to the injection spectrum required to explain the measured cosmic ray spectrum prior to steepening due to propagation effects.

In spite of this apparent success, observational difficulties for the hypothesis that cosmic rays are accelerated by SNe bear repeating (Dermer, 2000)

- The unidentified EGRET γ-ray sources have not yet been firmly associated with SNRs and do not display distinct π^0 features (Esposito et al., 1996);
- The spectrum of the diffuse galactic γ-ray background is harder than is expected if the locally observed cosmic ray proton and ion spectrum is similar throughout the Galaxy (Hunter et al., 1997);
- The acceleration of particles above the knee of the cosmic ray spectrum is difficult to explain in the simplest theory (Lagage and Cesarsky, 1983) of cosmic ray acceleration by SNRs; and
- As we have seen, TeV radiation is not detected at the expected levels.

In view of these difficulties, it seems possible that cosmic rays are predominantly accelerated by the subset of SNe which eject relativistic outflows. Bright enhancements of hadronic emission from those SNe which host GRB events are implied. From the rate estimates shown in Table 1, we see that about 1 in 20 to 1 in 100 SNRs would exhibit this enhanced emission. The better imaging and sensitivity of the *GLAST* telescope and the next generation of ground-based air Cherenkov telescopes will be able to test this hypothesis.

7 High Energy Neutrons and Neutrinos from GRBs

Observations of neutral particles and their secondary radiations will test the hypothesis that cosmic rays are accelerated by GRB blast waves. Neutron-decay halos are formed around galaxies that harbor GRB activity (Dermer, 2000). Equation (35) shows that the sources of GRBs inject a mean power of $10^{40\pm1}$ ergs s^{-1} into a typical L^* galaxy. In order to explain the locally observed UHECR energy density, each GRB source must accelerate ions with high efficiency. Neutrons will be directly produced through the process $p+\gamma\rightarrow n+\pi^+$ in the GRB blast wave and will escape the acceleration site. The neutrons, unbound by the magnetic field in the blast wave, leave the acceleration site with Lorentz factors $\gamma_n = 10^{10}\gamma_{10}$, where $0.1\lesssim\gamma_{10}\lesssim 100$. The neutrons decay on a timescale $\gamma_n t_n \cong 3\times10^5\gamma_{10}$ yrs, where the neutron β-decay lifetime $t_n\cong 900$ s.

The neutrons travel a characteristic distance $\lambda_n\cong 90\gamma_{10}$ kpc before they decay into highly relativistic electrons and protons. The electrons initiate an electromagnetic cascade that forms a diffuse $\approx$ 10 TeV Compton γ-ray component

and a nonthermal synchrotron component extending to soft γ-ray energies. The halo is unfortunately very weak. Three orders of magnitude reduction in the injection luminosity results from The β-decay to an electron results in three orders of magnitude reduction of power, and a further reduction results from the efficiency of photomeson production in the GRB blast wave. In an external shock model, the efficiency can be lower than 1%, implying powers of neutron decay radiation halos surrounding L^* galaxies at $\sim 10^{35}$ ergs s^{-1}.

Will water and ice Cherenkov neutrino telescopes detect GRBs in the light of high-energy photohadronic neutrinos? The comoving photon energy density is

$$\epsilon' u'(\epsilon') \cong \frac{d_L^2}{2cr_b'^{\,2}}\,\frac{f_\epsilon}{\Gamma^2}\ ,\ \text{and}\ \epsilon \cong \frac{2\Gamma\epsilon'}{1+z} \tag{37}$$

for a blast-wave geometry. The proper-frame density increases by 4Γ upon crossing a relativistic shock. The invariance of the total number of particles implies that $N = x^2(\Delta\Omega)\Delta'_{sh}n' = (\Delta\Omega)n_0\int_{x_0}^{x} d\bar{x}\bar{x}^2$, so that

$$r'_b \cong \Delta'_{sh} = \frac{x^3 - x_0^3}{12\Gamma x^2} \rightarrow \begin{cases} \frac{x}{12\Gamma}, & \text{uniform CBM} \\ \frac{x-x_0}{4\Gamma}, & \frac{x-x_0}{x_0} \ll 1 \end{cases} . \tag{38}$$

The comoving photon density is $n'(\epsilon') = \epsilon' u'(\epsilon')/m_e c^2 \epsilon'^{\,2}$, and the synchrotron emission is assumed to be isotropic in the comoving frame, so that $n'(\epsilon',\mu') \cong \frac{1}{2}n'(\epsilon')$.

The time scale for significant energy loss by photohadronic reactions is

$$t'^{\,-1}_{p\gamma\to\pi} \simeq \frac{c}{5}\int_0^\infty d\epsilon' \int_{-1}^{1} d\mu'(1-\mu')n'(\epsilon',\mu')\sigma_{p\gamma\to\pi}(\epsilon'') \ , \tag{39}$$

where $\sigma_{p\gamma\to\pi}(\epsilon'') \cong \sigma_0\delta[\mu' - (1-\epsilon_\Delta/\gamma'_p\epsilon')]$, $\sigma_0 \approx 2\times 10^{-28}$ cm^2, $\epsilon_\Delta \approx 640$, $\epsilon'' = \gamma'_p\epsilon'(1-\mu')$, and we now use primes to refer particle Lorentz factors to their proper frame. The comoving time available to undergo hadronic reactions is $t_{ava} \cong r'_b/c \cong 2\Gamma t/(1+z)$. The quantity

$$\eta \equiv \frac{t'_{ava}}{t'_{p\gamma\to\pi}} \cong \frac{\sigma_0 d_L^2\epsilon_\Delta}{20\gamma'_p m_e c^3\Gamma^2 r'_b}\int_{\epsilon_\Delta/2\gamma'_p}^{\infty} d\epsilon'\ \epsilon'^{-3}\ f_\epsilon \tag{40}$$

represents an efficiency for converting accelerated particle energy into neutrinos. The threshold condition $\gamma'_p\epsilon' \cong \epsilon_\Delta$ requires acceleration of protons with observer-frame energies $\gamma_p \cong \Gamma^2\epsilon_\Delta/[(1+z)\epsilon_{pk}] \propto \Gamma^{-2} \propto t^{3/4}$ from scattering with photons at the νF_ν peak photon energy ϵ_{pk}. As can be seen, demands on particle acceleration are more easily satisfied during the prompt phase of the GRB. Neutrinos are formed in the observer's frame with energies of $\approx 0.05 m_p c^2\gamma_p$. The peak photon energy of the νF_ν spectrum is

$$\epsilon_{pk} \cong \frac{2\Gamma}{(1+z)}\epsilon_B\gamma_{min}^2 \cong \frac{500}{1+z}\ k_p^2 e_e^2 (e_B n_0)^{1/2}\Gamma_{300}^4 \ . \tag{41}$$

The brightest neutrino production episode occurs $t \approx t_d$ for a fast cooling scenario, as can be shown from equation (40). Quantities evaluated at t_d wear hats. Equations (13) and (15) or rule (18) (Dermer et al., 1999a) imply

$$\hat{f}_{\epsilon_{pk}} \simeq \frac{2\Gamma^2}{4\pi d_L^2}\,(\frac{B^2}{8\pi}c\sigma_{\rm T})\ N_e^0\gamma_c\gamma_{min} \simeq \frac{3}{2}\,\frac{k_p e_e E_0}{4\pi d_L^2 t_d}$$
$$\simeq 10^{-6}\ \frac{E_{52}^{2/3}\Gamma_{300}^{8/3}n_0^{1/3}k_p e_e}{d_{28}^2(1+z)}\ \frac{\rm ergs}{\rm cm^2 s}\ , \tag{42}$$

so $\hat{f}_\epsilon = \hat{f}_{\epsilon_{pk}}(\epsilon/\hat{\epsilon}_{pk})^{\alpha_\nu}$ and $\alpha_\nu = 1/2$ for $\epsilon \le \hat{\epsilon}_{pk}$, $\alpha_\nu = (2-p)/2$ for $\epsilon > \hat{\epsilon}_{pk}$ in the fast cooling limit. From eq. (40),

$$\hat{\eta} \simeq \frac{\sigma_0 d_L^2\epsilon_\Delta\hat{f}_{\epsilon_{pk}}}{5\gamma'_{pk}m_e c^3(1+z)^2\hat{\epsilon}_{pk}^2 r'_b}\int_{\hat{y}_{pk}}^{\infty} dy\ y^{\alpha_\nu - 3}\ . \tag{43}$$

At $\hat{y}_{pk} = 1$, where $\alpha_\nu = \alpha_{\nu,u} = (2-p)/2$,

$$\hat{\eta}_{fc} \simeq \frac{\sigma_0 d_L^2\hat{f}_{\epsilon_{pk}}}{5(2-\alpha_{\nu,u})f_\Delta x_d m_e c^3(1+z)\hat{\epsilon}_{pk}}$$
$$\simeq \frac{10^{-2}}{(2-\alpha_{\nu,u})(1+z)f_\Delta}\ \frac{n_0^{1/6}E_{52}^{1/3}\Gamma_{300}^{-2/3}}{k_p e_e e_B^{1/2}}\ , \tag{44}$$

letting $r'_b = f_\Delta x_d/\Gamma$.

The low efficiencies of neutrino production makes detection of GRBs with a 1 km^3 neutrino telescope extremely unlikely within the context of a *uniform* external shock scenario (Dermer, 2000). Low Lorentz-factor dirty fireballs have increased efficiencies $\hat{\eta}_{fc}$ by as much as three orders of magnitude, but require acceleration to $\gamma_{pk} \simeq 10^{10}/\Gamma_0^2 k_p^2 e_e^2\sqrt{e_B n_0}$, which follows from the relation $\hat{y}_{pk} = \Gamma_0^2\epsilon_\Delta/\gamma_{pk}(1+z)\hat{\epsilon}_{pk} = 1$. The fast-cooling condition $\gamma_c < \gamma_{min}$ implies $e_e e_B \gtrsim 4\times 10^{-5}/[E_{52}^{1/3}n_0^{2/3}k_p(1+z)\Gamma_{300}^{4/3}]$, which additionally shrinks available parameter space.

Result (44) gives the photomeson production efficiency at the deceleration time scale for a proton with energy $m_p c^2\gamma_{pk} \simeq 10^{14}$ eV$/[k_p^2 e_e^2\sqrt{e_B n_0}\ \Gamma_{300}^2]$ eV in a fast cooling blast wave. Secondary neutrinos with energy $\sim 15\% \times m_p c^2\gamma_{pk}$ would be received from such GRBs. Deep water (Baikal, Nestor, Nemo, Antares) and ice (AMANDA, IceCube) neutrino detectors have detection probability $P \sim 10^{-4}P_{-4}$, with $P_{-4} \sim 1$ at PeV neutrino energies. The number of detected neutrinos N_ν can be approximated by the product of the telescope area $10^{10}A_{10}$ cm^2, the neutrino flux $\cong 10^{52}E_{52}$ $/[4\pi d_L^2(m_p c^2\gamma_{pk})]$ cm^{-2} s^{-1}, the multiplicity $3/2$ for muon neutrinos, and a bandwidth correction factor $0.1\zeta_{-1}$. The threshold energy for photomeson production by protons interacting with photons at the peak of the νF_ν synchrotron spectrum at $t = t_d$ is given by $m_p c^2\gamma_{pk} \cong m_p c^2\Gamma_0^2\epsilon_\Delta/[(1+z)\hat{\epsilon}_{pk}] \cong 170$ ergs$/[k_p^2 e_e^2\sqrt{e_B n_0}\ \Gamma_{300}^2]$.

Multiplying these factors together gives an estimate of the number of neutrinos that would be detected from a GRB, assuming that a comparable amount of energy is in the nonthermal proton spectrum as in the explosion:

$$N_\nu \simeq 4\times 10^{-4}\ \frac{A_{10}P_{-4}E_{52}^{4/3}k_p e_e n_0^{2/3}\Gamma_{300}^{4/3}\zeta_{0.1}}{d_{28}^2(2-\alpha_{\nu,u})(1+z)f_\Delta}\ . \tag{45}$$

Equation (45) is consistent with the numerical calculations of Dermer (2000), but much less accurate by neglecting the

energy dependence of P, and neutrino production in the afterglow phase. This result shows that there is no prospect for detecting $\gtrsim 1$ neutrinos from FRED-type GRBs, and we verify the computations (Dermer, 2000) of the weak neutrino flux produced by GRB blast waves decelerating in a uniform CBM.

Equation (45) says that GRBs are much brighter ν sources when $\Gamma_{300} \gg 1$, $n_0 \gg 1$, and $f_\Delta \ll 1$. Clean fireballs are however rare (Böttcher and Dermer, 2000). Density inhomogeneities from the SN envelope in the supranova model could enhance ν production in an external shock model, not only through the density effect indicated in equation (45), but through photo-hadronic processes with external photons (Atoyan and Dermer, 2001) and back-scattered photons. Eq. (38) shows that thin shells are formed in a clumpy medium, so that f_Δ could be $\ll 1/12$.[1] Because spiky and highly variable GRBs are due to large density contrasts in the external shock model on a size scale $\ll x/\Gamma$ (Dermer and Mitman, 1999), it seems possible that the spikiest and most variable GRBs could produce detectable high-energy ν emission in an external shock model. A definitive statement must await further studies.

Internal shock-model advocates (Waxman, 1995; Waxman and Bahcall, 1997) determine the blast-wave width from the observed variability time scale $t_{var} \simeq (1+z)r'_b/(c\delta)$, so that $r'_b = f_\Delta x/\Gamma \cong 2c\Gamma t_{var}/(1+z)$. Thus $f_\Delta \simeq t_{var}/t_d$, that is, the shell must lie within a distance $ct_{var} \ll ct_d$ of the central source, where the deceleration time t_d is associated with any surrounding CBM. Sufficiently small shell widths, though larger than the size scale of the original explosion, can enhance ν production considerably, so that the observable γ-ray power sets the only available scale on energy release. Pair attenuation in these inner regions will make γ-γ spectral cutoffs in the GLAST energy range. Studies of γ-γ opacity during the prompt phase of an external shock model find transparency up to TeV energies (Dermer et al., 2000a).

In the uniform external shock model, as we have seen, a very low efficiency for neutrino production is a consequence of the low radiation energy density in the comoving frame (Dermer, 2000). In models involving internal shocks, by contrast, the neutrino production efficiency can be much higher due to the larger radiation density (Waxman and Bahcall, 1997, 2000). In the latter case, GRBs should be detectable with km^3 scale neutrino detectors if UHECRs are indeed accelerated by GRB blast waves. Photon emission from the reverse shock can also enhance neutrino emission (Dai and Lu, 2001). Neutron decoupling from protons in the expanding fireball can also produce a strong flux of 5-10 GeV neutrinos (Bahcall and Mészáros, 2000). Secondary production can also be effective for high-energy neutrino production (Schuster et al., 2001).

We think that no measurable neutrino flux will be detected from smooth-profile GRBs. Spiky GRBs could be neutrino-bright, that is, potentially detectable in a km^3-scale experiment. It will be important to have continuous sky coverage with a GRB/hard X-ray survey instrument as IceCube and the northern hemisphere water arrays accumulate data.

[1] This answers a criticism of the external shock model posed by R. Sari.

8 Advanced Blast Wave Theory

All aspects of GRB theory cannot be treated in a short review, but at least some mention should be made of the main subjects overlooked. The physics of colliding shells in an internal shock/wind scenario was omitted, in keeping with Ockam's razor: *"pluralitas non est ponenda sine neccesitate,"* that is, "entities should not be multiplied unnecessarily." This hypothesis is not needed in GRB research; for an opposite viewpoint, see Piran (1999), and for a balanced assessment, see Mészáros (2002). (Colliding shell physics is of course important in black-hole jet studies; see, e.g., Spada et al. (2001).)

The physical approach summarized here has been developed by dozens of authors, and represents a generalization of supernova remnant physics to explosions with relativistic ejecta. Some important early contributions leading to the relativistic synchrotron-shock model include the works of Katz (1994) and Tavani (1996). A departure from a nonthermal synchrotron origin for the prompt emission is made by Lazzati et al. (2000) and Ghisellini et al. (2000), who argue that it is instead due to bulk Compton upscattering in a high photon energy-density region in the funnel of an exploding star. Part of the motivation for their work was observations of very hard X-ray emission with νF_ν indices $\alpha_\nu \gtrsim 2$ during the prompt γ-ray luminous phase of 5-10% of GRBs (Crider, et al., 1997; Preece et al., 1998). This strongly contradicts the optically-thin synchrotron shock model, which predicts that only spectra with $\alpha_\nu \leq 4/3$ can be radiated in a nonthermal synchrotron model.

Elaborations on the synchrotron-shock theory that may account for such hard spectra include photospheric emission (Mészáros and Rees, 2000) and radiation reprocessing by a medium heated by the γ rays (Dermer and Böttcher, 2000). These latter effects could lead to sites of enhanced annihilation radiation in the ISM at the location of GRB remnants, which INTEGRAL could discover. Madau and Thompson (2000) and Thompson and Madau (2000) treated Compton-backscatter effects from evolving γ-ray photon fronts, though initially approximated as an $\sim$10-100 lt-s shell of photons. The Compton back-scattered photons provide targets for successive waves of incident GRB photons through $\gamma\gamma$ pair-production interactions. Beloborodov (2001) and Mészáros et al. (2001) consider how pair-loading and preacceleration ("surfing") of the medium ahead of the γ-ray light front can alter the early afterglow and produce a bright optical/UV emission component during the early phases of a GRB. These early optical flashes might have been mistaken for a reverse shock emission. Paczyński (2001) suggests that these effects could produce optical flashes preceding a GRB.

Finally, we note that the theory of the central engine and gravitational radiation from GRBs is not treated here.

9 Conclusions

The Introduction summarizes the scope of this review, and will not be repeated here. The themes that I have tried to stress, and that would not have been possible to include in a review written only a year ago, are the implications of afterglow studies and X-ray absorption and line observations on source models. In particular, the constant energy reservoir result of Frail et al. (2001), derived by modeling breaks in GRB afterglow light curves, implies that GRBs are much more numerous and much less energetic than earlier believed. GRB sources are probably related to an unusual type of supernova occuring at $\sim$ 1% of the rate of Type II SNe, with energy releases several times greater than Type Ia or Type II SNe. Relativistic shock waves can accelerate particles to the ankle of the cosmic ray spectrum through second-order Fermi processes, so that cosmic rays between the knee and ankle of the cosmic ray spectrum could originate from GRB sources. If relativistic shocks accelerate particles with much greater efficiency than nonrelativistic shocks, then GRB sources could make a significant contribution to the production of cosmic rays with energies from GeV/nuc to the knee.

Cosmic rays may originate from the subset of supernovae that eject relativistic outflows. Gamma-ray observations with GLAST and ground-based air Cherenkov observatories will be fundamentally important to identify the sources of cosmic rays by searching for hadronic emission from discrete sites in the Galaxy. The Swift Observatory, in conjunction with ground-based followup, will establish a large database from which GRB redshifts, energies, and beaming fractions will be obtained. Neutrino observatories may force GRB source models to be revised. We look forward to further advances that will make this review obsolete.

Acknowledgements. I thank E. Ramirez-Ruiz, N. Trentham, D. Lazzati, M. J. Rees, P. Mészáros, M. Vietri, R. Schlickeiser, E. Waxman, and especially M. Böttcher for conversations and e-mail correspondence in preparation for this talk and during the completion of this review. The usual disclaimer applies: all errors are my own.

This work is supported by the Office of Naval Research and the NASA Astrophysics Theory Program (DPR S-13756G).

References

Akerlof, K., et al. 1999, Nature, 398, 400
Amati, L., et al. 2000, Science, 290, 953
Antonelli, L. A. et al. 2000, Astrophys. J., 545, L39
Atoyan, A., and Dermer, C. D. 2001, Phys. Rev. Letters, 87, 221102
Atkins, R. et al. 2000, Astrophys. J., 533, L119
Aharonian, F. A. et al. 2001, Astron. Astrophys., 370, 112
Bahcall, J. N. and Mészáros, P. 2000, PRL, 85, 1362
Band, D. et al. 1993, Astrophys. J., 413, 281
Beloborodov, A. M., 2001, ApJ, in press (astro-ph/0103321)
Bhat, P. N., Fishman, G. J., Meegan, C. A., Wilson, R. B., Brock, M. N., and Paciesas, W. S. 1992, Nature, 359, 217
Blandford, R. D., and McKee, C. F. 1976, Phys. Fluids, 19, 1130
Bloom, J. S., et al. 1999a, Astrophys. J., 518, L1
Bloom, J. S., et al. 1999b, Nature, 401, 453
Böttcher, M., Dermer, C. D., Crider, A. W., and Liang, E. P. 1999, Astron. Astrophys., 343, 111
Böttcher, M., and Dermer, C. D. 2000, Astrophys. J., 529, 635; (e) Astrophys. J., 536, 513
Böttcher, M., and Dermer, C. D. 2000, Astrophys. J., 532, 281
Böttcher, M., Fryer, C. L., and Dermer, C. D. 2002, Astrophys. J., 567, in press (astro-ph/0110625)
Buckley, J. H., et al. 1998, Astron. Astrophys. 329, 639
Catelli, J. R., Dingus, B. L., and Schneid, E. J. 1998, in Gamma-Ray Bursts, eds. C. A. Meegan, et al. (AIP: New York), 309
Cappellaro, E., Evans, R., and Turatto, M. 1999, A&A, 351, 459
Cheng, K. S. and Dai, Z. G. 1996, Phys. Rev. Letters, 77, 1210
Chiang, J., and Dermer, C. D. 1999, Astrophys. J., 512, 699
Ciardi, B. and Loeb, A. 2000, Astrophys. J., 540, 687
Costa, E. et al. 1997, Nature, 387, 783
Costa, E. 1999, Astron. Astrophys.S, 138, 425
Crider, A. et al. 1997, Astrophys. J., 479, L39
Dai, Z. G. and Lu, T. 2001, Astrophys. J., 551, 249
Dar, A., and De Rújula, A. 2000, astro-ph/0012227
Dar, A., and De Rújula, A. 2001, astro-ph/0110162
de Jager, O. C., et al. 1996, ApJ, 457, 253
Derishev, E. V., Kocharovsky, V. V., and Kocharovsky, Vl. V. 1999, Astrophys. J., 521, 640
Dermer, C. D. 2000, Astrophys. J., submitted (astro-ph/0005440)
Dermer, C. D. 2001, in the 27th Hamburg ICRC, 6, 2039
Dermer, C. D., and Mitman, K. E. 1999, Astrophys. J., 513, L5
Dermer, C. D., Chiang, J. and Böttcher, M. 1999, ApJ, 513, 656
Dermer, C. D., Böttcher, M., and Chiang, J. 1999, ApJ, 515, L49
Dermer, C. D., and Böttcher, M. 2000, Astrophys. J., 534, L155
Dermer, C. D., Böttcher, M., and Chiang, J. 2000, ApJ, 537, 255
Dermer, C. D., Chiang, J. and Mitman, K. E. 2000a, ApJ, 537, 785
Dermer, C. D., and Humi, M. 2001, Astrophys. J., 536, 479
Dermer, C. D., and Böttcher, M. 2002, in preparation
Djorgovski, S. G., et al. 1997, Nature, 387, 876
Djorgovski, S. G., et al. 2001, in Gamma Ray Bursts in the Afterglow Era, ed. E. Costa et al. (Springer: Berlin), 218
Drury, L. O'C. 1983, Rep. Prog. Phys., 46, 973
Efremov, Y. N., Elmegreen, B. G., and Hodges, P. W. 1998, Astrophys. J., 501, L163
Esposito, J. A., Hunter, S. D., Kanbach, G., and Sreekumar, P. 1995, Astrophys. J., 461, 820
Fishman, G. J. and Meegan, C. A. 1995, ARAA, 33, 415
Fowler, J. W., et al. 2001, Astroparticle Phys., 15, 49
Frail, D. A., et al. 1997, Nature, 389, 261
Frail, D. A. et al. 2001, Astrophys. J., 562, L55
Frontera, F., et al. 2000, Astrophys. J. S., 127, 59
Fryer, C. L. 2000, in Black Holes in Binaries and Galactic Nuclei, ed. L. Kaper et al., 2001 (Springer: New York), 328
Galama, T. J., et al. 1998, Astrophys. J., 500, L97
Gaisser, T. K. 1990, Cosmic Rays and Particle Physics (New York: Cambridge University Press)
Galama, T. J. and Wijers, R. A. M. J. 2001, Astrophys. J., 549, L209
Gallant, Y. A., and Achterberg, A., 1999, MNRAS, 305, L6
Ghisellini, G., Lazzati, D., Celotti, A., and Rees, M. J. 2000, MNRAS, 316, L45
Groot, P. J. et al. 1998, Astrophys. J., 493, L27
Heise, J. et al. 2001, in Gamma Ray Bursts in the Afterglow Era, ed. E. Costa, F. Frontera, and J. Hjorth (Springer: Berlin), 16
Huang, Y. F., Dai, Z. G., and Lu, T. 2002, MNRAS, in press (astro-ph/0112469)
Hunter, S. D., et al. 1997, Astrophys. J., 481, 205
Hurley, K. C., et al. 1994, Nature, 372, 652

Janka, H.-T., Eberl, T., Ruffert, M., and Fryer, C. L. 1999, Astrophys. J., 527, L39
Katz, J. I. 1994, Astrophys. J., 432, L107
Kirk, J.G., in Plasma Astrophysics (Saas-Fee 24th Advanced Course) (Berlin: Springer-Verlag), 225
Königl, A., Granot, J. 2001, ApJ, submitted (astro-ph/0112087)
Kouveliotou, C., et al. 1993, Astrophys. J., 413, L101
Krumholz, M., Thorsett, S., and Harrison, F. 1998, ApJ, 506, L81
Kulkarni, S. R., et al. 1998, Nature 395, 663
Lagage, P. O., and Cesarsky, C. J. 1983, A&A, 118, 223
Lamb, D. Q. and Reichart, D. E. 2000, Astrophys. J., 536, 1
Lazzati, D., Ghisellini, G., Celotti, A., and Rees, M. J. 2000, Astrophys. J., 529, L17
Lazzati, D., Ghisellini, G., Amati, L., Frontera, F., Vietri, M., and Stella, L. 2001, Astrophys. J., 556, 471
Lee, H. K., Brown, G. E., and Wijers, R. 2000, ApJ, 536, 416
Liang, E. and Kargatis, V. 1996, Nature, 381, 49
Loeb, A., and Perna, R. 1998, Astrophys. J., 503, L35
Lozinskaya, T. A. 1992, Supernovae and Stellar Wind in the Interstellar Medium (New York: AIP)
MacFadyen, A. I. and Woosley, S. E. 1999, Astrophys. J., 524, 262
MacFadyen, A., Woosley, S., and Heger, A. 2001, ApJ, 550, 410
Madau, P., Pozzetti, L., and Dickinson, M. 1998, Astrophys. J., 498, 106
Madau, P. and Thompson, C. 2000, Astrophys. J., 534, 239
Mallozzi, R. S., et al. 1995, Astrophys. J., 454, 597
Mallozzi, R. S., et al. 1997, in 4th Huntsville Symposium on Gamma-Ray Bursts, eds. C. A. Meegan, et al., p. 273
Marani, G. F., Nemiroff, R. J., Norris, J. P., Hurley, K., and Bonnell, J. T. 1999, Astrophys. J., 512, L13
McBreen, B., and Hanlon, L. 1999, Astron. Astrophys., 351, 759
Meegan, C. A., et al. 1992, Nature, 355, 143
Meegan, C. A., et al., 1996, Astrophys. J. S., 106, 65
Mészáros, P. 2002, ARAA, in press (astro-ph/0111170)
Mészáros, P., and Rees, M. J. 1993, Astrophys. J., 405, 278
Mészáros, P., Laguna, P., and Rees, M. J. 1993, ApJ, 415, 181
Mészáros, P. and Rees, M. J. 1997, Astrophys. J., 476, 232
Mészáros, P., Rees, M. J., and Wijers, R. 1998, ApJ, 499, 301
Mészáros, P. and Rees, M. J. 2000, Astrophys. J., 530, 292
Mészáros, P. and Rees, M. J. 2001, Astrophys. J., 556, L37
Mészáros, P., Ramirez-Ruiz, E., and Rees, M. J. 2001, Astrophys. J., 554, 660
Mészáros, P. and Waxman, E. 2001, Phys. Rev. Letters, 87, 1102
Metzger, M. R., et al. 1997, Nature, 387, 878
Milgrom, M., and Usov, V. 1995, Astrophys. J., 449, L37
Moderski, R., Sikora, M., and Bulik, T. 2000, ApJ, 529, 151
Murakami, T., et al. 1991, Nature, 350, 592
Narayan, R., Piran, T., and Shemi, A. 1991, Astrophys. J. 379, L17
Norris, J. P., Marani, G. F., and Bonnell, J. T. 2000, ApJ, 534, 248
Paczyński, B. 1998, Astrophys. J., 494, L45
Paczyński, B., and Rhoads, J. 1993, Astrophys. J., 418, L5
Paczyński, B., astro-ph/0108522
Panagia, N. 2000, in Experimental Physics of Gravitational Waves, ed. G. Calamai, et al. (World-Scientific: Singapore), in press
Panaitescu, A., Mészáros, P., and Rees, M. J. 1998, ApJ, 503, 314
Panaitescu, A., and Kumar, P. 2001, Astrophys. J., 554, 667
Pian, E., et al. 1999, Astron. Astrophys. S., 138, 463
Piran, T. 1999, Phys. Reports, 314, 575
Piro, L., et al. 1999, Astrophys. J., 514, L73
Piro, L., et al. 2000, Science, 290, 955
Pohl, M., and Schlickeiser, R. 2000, Astron. Astrophys. 354, 395
Preece, R. D. et al. 1998, Astrophys. J., 506, L23
Rachen, J., and Mészáros, P. 1998, Phys. Rev. D, 58, 123005
Ramirez-Ruiz, E., Merloni, A., and Rees, M. J. 2001, MNRAS, 324, 1147
Ramirez-Ruiz, E., Lazzati, D., and Blain, A. W. 2002, ApJ, 565, L9
Ramirez-Ruiz, E., Trentham, N., and Blain, A. W. 2002, MNRAS, 329, 465
Rees, M. J., and Mészáros, P. 1994, Astrophys. J., 430, L93
Rees, M. J., and Mészáros, P. 1992, MNRAS, 258, 41P
Rees, M. J. and Mészáros, P. 2000, Astrophys. J., 545, L73
Reichart, D. E. 1999, Astrophys. J., 521, L111
Reichart, D. E., et al. 2001, Astrophys. J., 552, 57
Rhoads, J. E. 1999, Astrophys. J., 525, 737
Ruffini, R., et al. 2001, ApJ, 555, L107
Sari, R., and Piran, T. 1995, Astrophys. J., 455, L143
Sari, R., Narayan, R., and Piran, T. 1996, Astrophys. J., 473, 204
Sari, R., Piran, T., and Narayan, R. 1998, Astrophys. J., 497, L17
Sari, R., Piran, T., and Halpern, J. 1999, Astrophys. J., 519, L17
Scalo, J., and Wheeler, J. C. 2002, ApJ, in press (astro-ph/9912564)
Schlickeiser, R., and Dermer, C. D. 2000, A&A, 360, 789
Schuster, C., Pohl, M., and Schlickeiser, R. 2001, A&A, in press (astro-ph/0111545)
Simpson, J. A. 1983, Ann. Rev. Nuclear and Particle Phys., 33, 323
Sokolov, V. V. et al. 2001, Astron. Astrophys., 372, 438
Sommers, P., oral contribution at Aspen Workshop on UHE Particles from Space (January 27 - February 2, 2002)
Spada, M., Ghisellini, G., Lazzati, D., and Celotti, A. 2001, MNRAS, 325, 1559
Stanev, T., Engel, R., Mücke, A., Protheroe, R. J., and Rachen, J. P. 2000, Phys. Rev. D, 62, 093005
Stecker, F. W., 2000, Astroparticle Phys., 14, 207
Takeda, M., et al. 1998, Phys Rev. Letters, 81, 1163
Tan, J. C., Matzner, C. D., and McKee, C. F. 2001, ApJ, 551, 946
Tavani, M. 1996, Physical Review Letters, 76, 3478
Thompson, C. and Madau, P. 2000, Astrophys. J., 538, 105
Totani, T. 1997, Astrophys. J., 486, L71
Totani, T. 1999, Astrophys. J., 511, 41
Tutukov, A. V., and Yungelson, L. R. 1993, MNRAS, 260, 675
Usov, V. V. 1992, Nature, 357, 472
Usov, V. V. 1994, MNRAS, 267, 1035
van Paradijs, J., Kouveliotou, C., and Wijers, R. A. M. J. 2000, Ann. Rev. Astron. Astrophys. 38, 379
van Paradijs, J., et al. 1997, Nature, 386, 686
Vietri, M. 1995, Astrophys. J., 453, 883
Vietri, M. 1997, Astrophys. J., 478, L9
Vietri, M. 1998, Astrophys. J., 453, 883
Vietri, M. 1998, Astrophys. J., 507, 40
Vietri, M. and Stella, L. 1998, Astrophys. J., 507, L45
Vietri, M. and Stella, L. 1999, Astrophys. J., 527, L43
Vietri, M., Perola, C., Piro, L., Stella, L. 1999, MNRAS, 308, L29
Völk, H. J. and Biermann, P. L. 1988, Astrophys. J., 333, L65
Waxman, E. 1995, Phys. Rev. Lett. 75, 386
Waxman, E. 1997, Astrophys. J., 485, L5
Waxman, E., and Bahcall, J. N. 1997, Phys. Rev. Lett. 78, 2292
Waxman, E., and Bahcall, J. N. 2000, Astrophys. J., 541, 707
Woosley, S.E. 1993, Astrophys. J., 405, 273
Weiler, K. W., et al. 2000, in Supernovae and Gamma-Ray Bursts, ed. M. Livio, N. Panagia, and K. Sahu, (astro-ph/0002501)
Wijers, R, Bloom, J., Bagla, J., Natarajan, P. 1998, MNRAS, 294, L13
Wijers, R. A. M. J., and Galama, T. J. 1999, Astrophys. J., 523, 177
Yoshida, A., et al., 1999, Astron. Astrophys.S, 138, 433
Zhang, B., and Mészáros, P. 2001, Astrophys. J., 559, 110